PL-TR--91-3111

PL-TR--
91-3111

(2)

CRITICAL TECHNOLOGY DEMONSTRATION OF PLASMA FOCUS TYPE MPD THRUSTER

George H. Miley
Johathan Nadler
Brian Temple
Scott Bolt
Hanoch Kislev

Rockford Technology Associates, Inc.
912 W. Armory
Champaign IL 61821

May 1992

Final Report

PHILLIPS LABORATORY
Propulsion Directorate
AIR FORCE SYSTEMS COMMAND
EDWARDS AIR FORCE BASE CA 93523-5000

NOTICE

When U.S. Government drawings, specifications, or other data are used for any purpose other than a definitely related Government procurement operation, the fact that the Government may have formulated, furnished, or in any way supplied the said drawings, specifications, or other data, is not to be regarded by implication or otherwise, or in any way licensing the holder or any other person or corporation, or conveying any rights or permission to manufacture, use or sell any patented invention that may be related thereto.

FOREWORD

This Final Report was submitted by Rockford Technology Associates, Inc. under SBIR Contract F29601-91-C-0036 with the OLAC, Phillips Laboratory, Edwards AFB CA 93523-5000. SBIR funding was provided by the Small Business Innovative Research Program. OLAC PL Project Manager was Franklin B. Mead Jr.

This report has been reviewed and is approved for release and distribution in accordance with the distribution statement on the cover and on the SF Form 298.

Franklin B. Mead Jr.

FRANKLIN B. MEAD JR.
Project Manager

Stephen L. Rodgers

STEPHEN L. RODGERS
Chief, Emerging Technologies Branch

LEONARD C. BROLINE, LT COL, USAF
Acting Director,
Fundamental Technologies Division

RANNEY G. ADAMS
Public Affairs Director

REPORT DOCUMENTATION PAGE

Form Approved
OMB No. 0704-0188

1. AGENCY USE ONLY (Leave blank)	2. REPORT DATE	3. REPORT TYPE AND DATES COVERED
	May 1992	Final Report 4 April - 4 October 1991

4. TITLE AND SUBTITLE

Critical Technology Demonstration of Plasma Focus Type MPD Thrusters

5. FUNDING NUMBERS

C - F29601-91-C-0036
PE - 62302F
PR - 3058
TA - 0096

6. AUTHOR(S)

George H. Miley; Jonathon Nadler; Brian Temple; Scott Bolt; Hanoch Kislev

7. PERFORMING ORGANIZATION NAME(S) AND ADDRESS(ES)

Rockford Technology Associates, Inc.
912 W. Armory
Champaign IL 61821

8. PERFORMING ORGANIZATION REPORT NUMBER

9. SPONSORING MONITORING AGENCY NAME(S) AND ADDRESS(ES)

Phillips Laboratory (AFSC)
OLAC PL/RKFE
Edwards AFB CA 93523-5000

10. SPONSORING MONITORING AGENCY REPORT NUMBER

PL-TR-91-3111

11. SUPPLEMENTARY NOTES

COSATI Codes: 18/01; 20/08; 20/09

12a. DISTRIBUTION/AVAILABILITY STATEMENT

Approved For Public Release; Distribution Unlimited

12b. DISTRIBUTION CODE

13. ABSTRACT (Maximum 200 words)

The technical objective of the Phase I work was to study the optimization and scaling of a plasma focus type MPD thruster device in order to design a MJ-scale test facility for construction in Phase II. This report describes studies done to develop the capacitor bank and electrode design for the MJ facility. A modular design is proposed which would allow construction and testing of a 1/4-MJ facility in Phase II with the addition of the remaining modules to be done in Phase III. Details of thruster electrode design studies for use in the 1/4-MJ device and the facility specifications are given in this report. Key items include a fast gas-injection system, control system and timing circuits, advanced target design concepts, and switching circuits.

14. SUBJECT TERMS	15. NUMBER OF PAGES
Plasma thruster, plasma focus, MPP, D-^{3}He fusion	80
	16. PRICE CODE

17. SECURITY CLASSIFICATION OF REPORT	18. SECURITY CLASSIFICATION OF THIS PAGE	19. SECURITY CLASSIFICATION OF ABSTRACT	20. LIMITATION OF ABSTRACT
UNCLASSIFIED	UNCLASSIFIED	UNCLASSIFIED	SAR

Table of Contents

List of Figures

List of Tables

CRITICAL TECHNOLOGY DEMONSTRATION OF PLASMA FOCUS TYPE MPD THRUSTER

Introduction

Phase I of this study had three objectives, namely:

a) Design and test of various electrode designs.
b) Design a 1 MJ DPF facility.
c) Perform a cost study for scaling up to a 1 MJ facility.

Results from work on each objective are summarized below. We have met the objectives specified, although some minor variations were found to be necessary and were implemented with consent of the project monitor.

a) A decision was made earlier during this project (with consent of the contract monitor) to expand the theoretical studies of the electrode designs for Phase II and delay specific experimental studies until that phase. This approach has the advantage that a much wider variety of designs could be considered without an excess expenditure of funds and time. With the design options narrowed in this fashion, the testing during Phase II will be more cost effective.

   Over 20 different electrode designs were rigorously studied under various operating conditions. Results from these studies are described in detail in Section III. On the basis of this study, a "best" design was selected for detailed mechanical design and construction for testing in Phase II.

b) A 1-MJ facility design has been studied in detail. Rockwell's Plasma Focus research team, in consultation with Maxwell Corporation, have concluded that due to present data and technology limitations, an intermediate scaling to 1/4-MJ is the most logical next step for Phase II. This 1/4-MJ system has been designed to be modular and therefore easily expandable to a 1-MJ facility. This modular design will reduce future expansion costs, and allow for relatively easy updating of DPF components as new technology evolves.

   The development plan then consists of using 1/4-MJ steps to build up to 1-MJ. This approach, combines theory and experiment, at each step will provide a sound basis for scaling up to a yet larger prototype device. Thus, based on discussions with AF scientists, we propose that ultimate prototype thruster studies of the latter be carried out using Rockford electrode designs in the 9-MJ pulsed power facility located at the Phillips Laboratory in Albuquerque, NM.

c) Technical and cost studies have been performed for both the modular 1/4-MJ unit and a full scale MJ device. These studies indicate the need for intermediate scaling prior to undertaking 1-MJ experiments. The lack of sufficient scaling data for a 1-MJ unit with gas puff injection mandates the need for intermediate scaling data. Scaling directly to 1 MJ would be exceedingly costly and potentially risky without such tests. Consequently, the design for a first step 1/4-MJ facility is given in section IV.

Additional key components necessary for successful operation of the 1/4- and 1-MJ facilities were studied in Phase I. These include the design of the gas injection system (Sec. IV), the control/timing circuit (Sec. V), and an advanced target concept to increase the energy gain (Sec. VI). Results from these studies are presented here and a complete description of the proposed facility will be provided in the Phase II proposal for this project.

Background

Importance, Propulsion Applications. This contract was initiated to determine the feasibility of a 1-MJ scale facility needed to qualify the Dense Plasma Focus (DPF) as a suitable candidate for use as a space thruster. The need exists for a simple, light-weight, high-specific impulse, high-power density thruster for Air Force missions. If the DPF can fulfill these requirements, current Air Force missions might be enhanced (e.g., orbit station propulsion, orbit transfer), and previously unattainable missions (e.g., Mars transfer) might be enabled.

The DPF shows very promising characteristics with regards to the propulsion requirements listed above. It offers a (1) compact, small size; (2) simple, co-axial geometry; (3) high-velocity rundown of gas/plasma (high specific impulse); (4) the addition of fusion energy which greatly reduces the energy storage/recirculation needed for a standard MPD thruster.

Electric propulsion is not new to the Air Force; it is characterized by very high specific impulse (I_{sp}~1000 s) and very low thrust (F~10 N), typical of arc-jet and Magneto-Plasma-Dynamic (MPD) devices. Indeed, the coaxial electrode configuration of the DPF is quite similar to the MPD device. However, a major advantage of the DPF comes from the fusion contribution to the output energy and the high specific impulse from the arc rundown. When the plasma sheath collapses at the end of the cathode, the plasma trapped inside is brought to temperatures and densities high enough for significant fusion to occur (Y_n~10^{12} DD fusion

events/shot recorded by Frascati 1-MJ experiment[1]). The arc-jet and MPD devices do not pinch the plasma in this manner, and thus are not able to take advantage of added fusion energy.

Preliminary estimates, summarized in Appendix A, indicate that, with advances in the state of the art, the ratio of (fusion energy/bank energy delivered to the pinch) might approach fifty percent. This would result in a very significant reduction in the recirculating/storage energy requirement, greatly enhancing the power to weight ratio for such devices.

For the present Rockford studies, experimental verification of rocket performance is the ultimate goal. Thus gas is injected at the base of the electrodes from a plenum. The gas is ionized and accelerated down the electrodes to the end. At the end, when the sheath collapses, a fraction of the gas is trapped in the pinch, while the remainder is exhausted axially (producing thrust). The fusion energy released in the pinch is rapidly thermalized in the high density plasma. A variable impulse-thrust ratio can then be obtained by mixing this hot exhaust plasma with an appropriate propellant fluid such as hydrogen.

State of the Art. An extensive volume of both theoretical and experimental work was done on the plasma focus. However, little is known about a gas-injected focus of the type desired for space applications.

Rockford researchers have collected and reviewed the available information in order to determine the key issues and work necessary for the scale-up and testing proposed for Phase II. Some highlights are outlined here.

a) Theoretical Studies. Maxon[2], Potter[3], and Kondoh and Hirano[4] have performed numerical calculations modelling the DPF. Temperatures on the order of several 10's of keV are predicted for a 5-MJ DPF, thus significant fusion should occur at these energy levels[2]. However, MHD theory breaks down at these energies so experimental confirmation remains essential[2].

Much attention has been devoted to the matching of rundown and pinch impedance to the impedance of the capacitor bank at the time of maximum current delivery[1,5]. This is done to avoid transmission line-like reflection, as well as prevent re-strike of the plasma arc at the base of the electrodes during the pinch time. Information from these studies has been heavily used in our electrode design studies.

b) Experimental Studies. In addition to the 15-kJ bank at the U. of Illinois (rented by Rockford for present studies), there are several facilities around the world that have operating DPF devices (Stevens Inst. of Tech., Los Alamos National Lab, Phillips Laboratory, IPF (Stuttgart), IPJ (Swierk), Kurtmallov Inst., etc.). The research goal of the majority of these facilities is to increase the measured neutron yield Y_n, which is an indicator of the fusion reactions occurring. If Yn is increased, the promise of the device is improved as a commercial 2.45-Mev neutron source, and perhaps even a commercial power source. All of these devices operate with a static fill, however. Thus it is essential to obtain experimental data for gas injected DPF's, starting at ~ 1/4 MJ and scaling up.

Experimental DPF devices range in geometry[6] (Mather vs. Fillipov), insulator material (ceramic, Pyrex), and capacitor bank energy (1/4-kJ-1-MJ)[5,7], but none of them are designed to measure thrust directly, as the Rockford design will. Gates[8] also performed simultaneous gas injection directly into the pinch from the end of the cathode during rundown (to artificially increase the high-Z ion fraction without sacrificing rundown performance)[8]. This approach was successful but does not quite provide the geometry desired for propulsion. Still these results provide considerable confidence that a gas-injected device for propulsion can be developed.

Impedance Matching, Restrike. As mentioned above, matching the impedance of the pinch to the impedance of the capacitor bank and the time of maximum current delivery is critical to successful operation of the DPF. If the bank and pinch are not matched, energy will be "reflected" from the pinch, inducing a plasma arc in a region of lower impedance (across the insulator) and reducing energy delivered to the pinch. Little detailed information about these issues is available in the literature. Thus, to study this issue, we have developed an improved model of the impedance and current during rundown. This model is incorporated in a computer code, described later in Sec. IV which combines the arc rundown physics with an equivalent RLC circuit for the pulsed power supply. Matching impedances for the pinch is made difficult by the uncertainty inherent in available theoretical models of the pinch impedance as a function of time, current, bank energy, and electrode geometry. This uncertainty arises because "shunt current" from the restrike represents major loss of energy delivered to the pinch at higher bank energies. Thus this represents a major scaling issue that will be studied with the 1/4-MJ device in Phase II.

These various impedance matching considerations have guided the design of the electrodes and of the bank switches

and the transmission lines for the Phase II design. The electrode designs are described next.

Electrode Design

Objectives. To maximize the DPF as a propulsion device, various electrode geometries can be used to enhance the arc rundown and pinch characteristics. Electrode geometries cannot be selected at random since each electrode configuration has a different impedance. The power delivery system and the load behave the same as two connected transmission lines. If the impedances do not match, then the system behaves as an under-damped or over-damped RLC circuit. Thus the system and load resistances must match to achieve efficient voltage transmission from the power delivery system to the load. If the reactance of the system and the added load do not cancel to zero, the current will be out of phase with the voltage. In summary then, the reactance of the system and the load must add together to equal zero for efficient voltage transmission.

The proposed Phase II device can be represented by an under-damped RLC circuit in which the small resistance of the electrodes creates an under-damped situation. It is impossible to reduce the system resistance or increase the electrode resistance so that these two elements match perfectly. Thus the only significant way to adjust the impedance to maximize power transmission is to alter the electrode inductance. In the present DPF design the load reactance cannot be adjusted to make the entire reactance zero. Thus the inductance of the electrode is made similar in magnitude to the inductance of the system. This choice of inductance makes the circuit decay constant of the DPF independent of the inductance of the entire system.

The inductance of the electrodes is also related to the ratio of the inner and outer electrodes. However, in order to obtain a desired gas density between the electrodes, the design must have adequate volume between the electrodes. Thus the electrode inductance is set by a trade-off that involves the desired gas volume between the electrodes.

To this point we have discussed conventional cylindrical type electrodes with a constant radius vs. length. However, to obtain an added run-down velocity, hence pinch density, tapered electrodes are an obvious alternative. Tapering the electrodes, however, greatly complicates the inductance calculation. Thus, to handle this, we have developed a modified version of a zero dimensional code derived for the UI DPF by J. Mandrekas[9]. This code solves the circuit equation for the system in static mode with the plasma focus represented by a time dependent inductance and resistance. The latter are then coupled to a momentum equation of motion for the arc plasma.

The modified Mandrekas code used in this work is described in detail in Appendix B.

These electrode design studies must be viewed as a first approximation for optimizing system performance in the gas-injected mode. The inductance values calculated from the modified Mandrekas code are valid for any mode of operation. Therefore impedance calculations can be performed for various electrode designs in the gas-injected mode. However, the axial velocity profiles given by the code are not completely accurate for gas-injected operation of the DPF.

A key objective of Phase II will be to test this modeling in preliminary studies at the 1/4-MJ level. This will provide a more accurate scaling and optimization for subsequent studies at higher energies. While prior DPF experiments have been performed elsewhere at these energies. These will be the first with a gas injected system. Thus the data obtained will be essential for the eventual development of a 1-MJ thruster.

DPF Run-down Computer Model. Mandrekas's original code was largely based on methods originally proposed by P. Elgroth[10]. A flow chart for the code is illustrated in Fig. 1 (Also see Appendix B for details). In order to solve these complex nonlinear equations, a variety of assumptions about the DPF mechanisms system are made. These assumptions are generally normalized to experimental results obtained from a DPF similar in size to the present 25-kJ DPF and combined with results from a two-dimensional code developed by Maxon and Eddleman[2]. The results of Elgroth's work has been shown to be within ten percent of predictions from Mason's code for a reasonable range of bank energies. Also results from the version developed by Mandrekas are within ten to fifteen percent of experimental data from the present DPF. However, all of these comparisons are based upon a DPF operated in the static mode. Thus, a comparison to a gas-injected system is essential and this will be one of the initial tasks carried out in Phase II.

Other key assumptions in the present run-down code include the postulate that the acceleration of the current sheath is negligible. For the gas-injected mode of operation this is probably accurate. When an arc rundowns between the electrodes in the static-filled mode, the gas particles pushed by the arc collide with the other static particles in the chamber. The static particles exert a back pressure on the arc as it runs up. Since the outer electrode for the DPF is not solid, the static gas equalizes itself out by flowing in back of the arc as it runs down the electrode. Thus the current sheath does not accelerate significantly since the back pressure exerted by the gas is

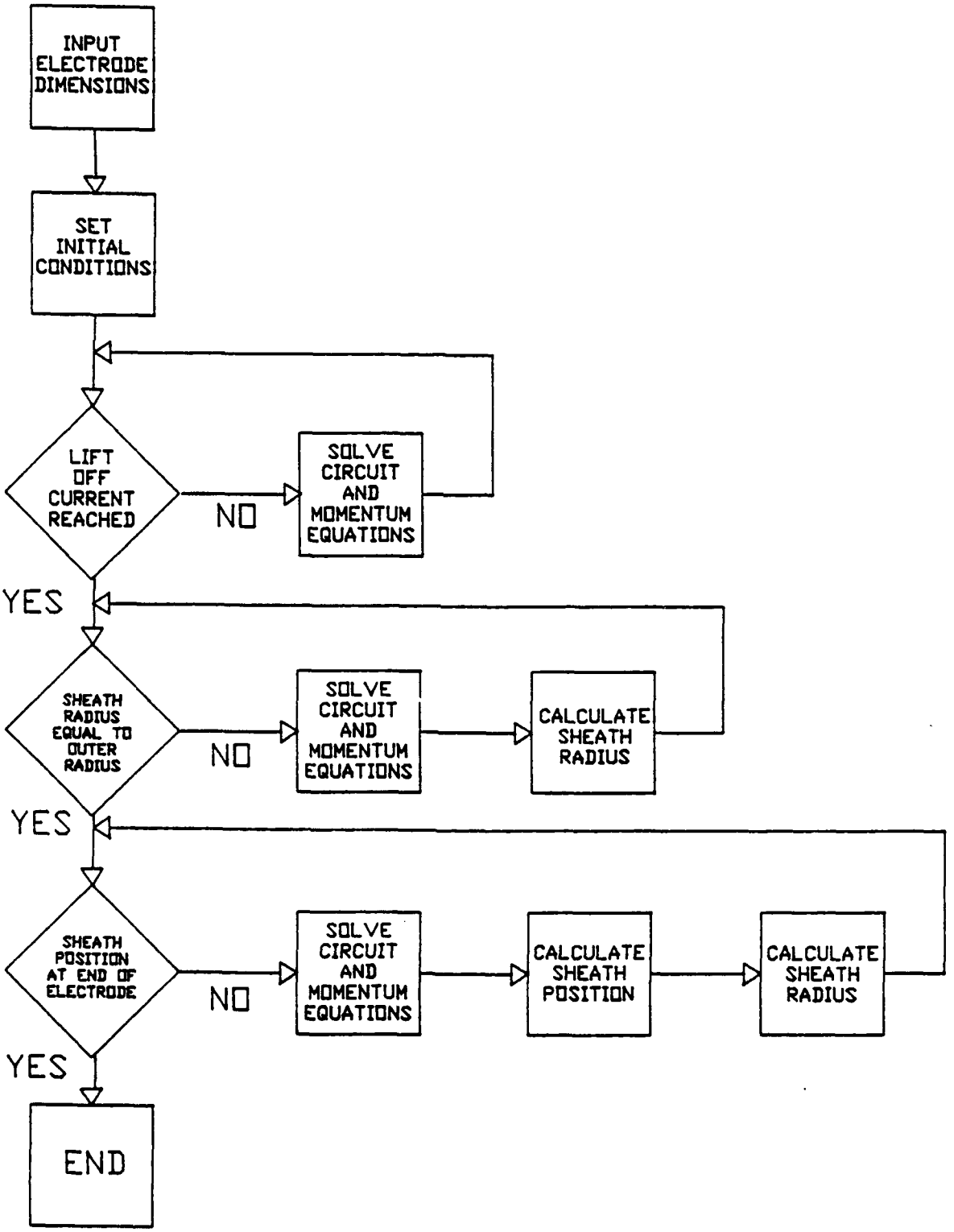

Figure 1

Flow Chart for the DPF Computer Model.

kept fairly constant by the equalization of the gas. In the gas-injected mode the arc will not experience the constant back pressure since the gas is injected into a vacuum. Some back pressure may occur from the inertia of the gas, but it will vary with the percentage of gas that is swept up by the arc. Therefore the final velocity of the arc should be faster in the gas-injected mode. We have not yet attempted to correct the code for this effect, however, since the error involved will be in a conservative direction, relative to present electrode designs. A correction will be incorporated later in Phase II when this code is benchmarked against experimental results.

The run-down code calculates the change of inductance with respect to time using a quasi-equilibrium approximation where the inductance vs. axial length calculation is employed corresponding to the arc position. This assumption is justified from the fact that experimental observation shows this to be true during arc rundown in the static mode. However if the electrode has an inner electrode radius that changes, the assumption is not strictly valid since the inductance is basically a function of the length of the electrodes and the ratio of the inner and outer radii. In the modified code the inductance is changed as a function of the axial position of the sheath. The radius of the electrode is held constant for the distance traveled by the arc in one time increment at the axial velocity calculated for the increment. Thus the change of inductance with respect to time is given by a chain rule, i.e., as the change of inductance with respect to axial position multiplied by the axial velocity of the arc. With this approach, the accuracy is limited by the time increment selected and by the axial velocity, i.e., by the available computer time.

In the circuit equation (corresponds to the circuit of Fig. 2) we assume that the plasma resistance is insignificant compared to the system resistance. In the present DPF the electrode resistance calculated with a vacuum between the electrodes is approximately 1000 times smaller than the system resistance. Thus this assumption should still hold true for the gas-injected mode. If this code were to be modified for use on a larger system with significantly smaller resistances, then the plasma resistivity will need to be calculated as the arc propagates between the electrodes.

A key ingredient that the modified run-down code lacks is the ability to account for the acceleration of the arc. However, a basic relationship that is common between the two modes of operation is that the increase in current and decrease in radius should cause an increase in the axial velocity of the rundown. This relation can be used with the work performed as a crude guideline in determining how

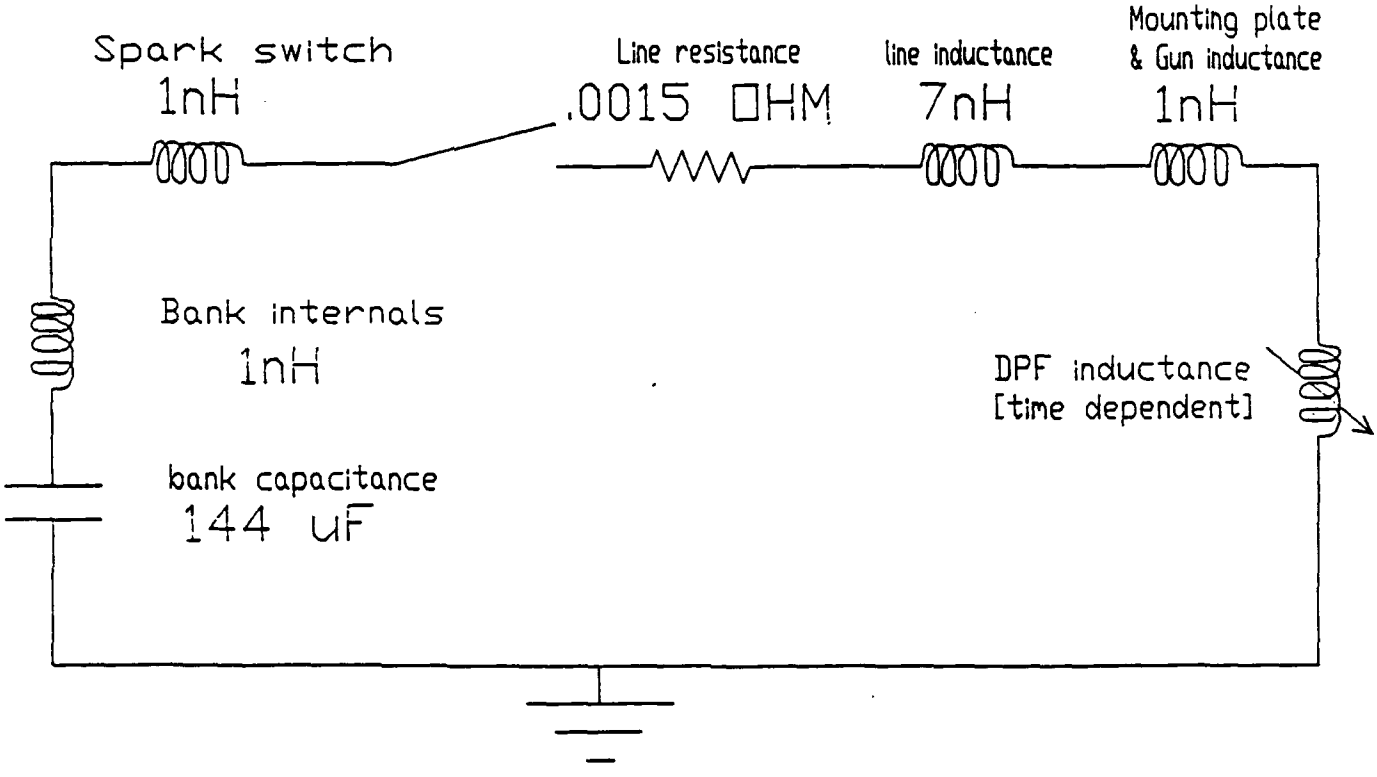

Figure 2

Equivalent Circuit Employed in the DPF Code.

electrode design can effect rundown parameters. Greater insight into the correlation between the rundown dynamics of the two modes of operation can be made once data is obtained from gas-injected experiments. A clear insight into the acceleration effects of the rundown in a gas injected system can then be determined. However at the present time, no strict conclusions from the velocity profiles produced from Mandrekas's modified code should be made.

The inductance of the electrode can be compared with the system inductance of the DPF. The inductance of the system is 24.5 nH. Electrode geometries which have a larger inductance than other geometries should have a smaller plasma current. This is evident from evaluation of the circuit equations. The smaller current will lead to a slower rundown time since the axial velocity is related to the current. Geometries which have a smaller inductance will have faster rundown times and higher currents due to the larger amount of current transferred to the electrodes. The axial velocity and inductance are inversely proportional to the inner electrode radius.

Electrode Design Studies. Fourteen basic electrode designs were run through the modified run-down code.

The various geometries considered can be generally broken into three groups assuming a 19.6 cm electrode length:

- Length of geometry change (i.e., length of taper, curved section, etc.)

  Geometry change begins at 18 cm.
  Geometry change begins at 12 cm
  Geometry change begins at 3.2 cm.

- Curvature of geometry change

  Inward (concave) curvature
  Outward curvature

- Final radius of electrode (2.54 cm initial radius)

  1 cm end radius
  2 cm end radius

Key designs selected from the 14 considered due to their good performance are illustrated schematically in Figs. 3-5. The first design represents a conventional cylindrical electrode with square corners. It is included as a reference case. The next three designs (#41-43) have the square ends removed, using various curvatures for their tips. The final three designs (#52-54) employ tapered geometries with various taper curvatures.

Calculations of the axial velocity verses time were performed to determine which inner electrode designs would give the maximum axial velocity and shortest rundown times. Graphs of the results for the electrodes shown in Figs. 3-5 are given in Figs. 6 and 7.)

The velocities for the various rounded tip designs are fairly similar until the plasma hits the tip (i.e., curvature) region where a rapid increase in velocity suddenly occurs. There is a wider spread in velocities for the tapered design, but the rapid increase in velocity at the end is avoided.

Another important characteristic for evaluating the electrode designs is the inductance vs. axial length, i.e., the time dependence of the inductance as the arc "runs down" the axis. The inductance-length graphs for the previous electrodes are shown in Figs. 8 and 9. It is seen that slowly tapered designs like designs 52, 53, and 54 increase the inductance by nearly an order of magnitude. Designs with a sharp curvature in the electrode had nearly the same inductance as the reference electrode (#40).

In summary, curved tip designs 41, 42, and 43 give the highest axial velocities possible with low inductance values. With sharp electrode curvatures at the end of the electrode, the inductance is kept low and a large current is obtained as the arc nears the end of the electrode. Tapered designs like 52, 53, and 54 have smaller radii at the end of the electrode, resulting in a slower rundown time than larger radius electrodes. The smaller overall average radii of these designs give a higher inductance and thus a smaller current as the arc nears the end of the electrode. This is not desirable so these designs are given a low rating due to this effect.

Based on these studies we conclude that the sharpness of the curvature is more important than the direction of curvature. Further, the curvature should occur toward the end of the rundown so the increase of inductance resulting from the smaller radius will not significantly decrease the current of the pulsed power system.

Taking all of these effects into account, we conclude that the best electrode design for static mode operation would be Design 41 (rounded tip, 1" curvature). This design has a large constant radius until the end of the end of the electrode where it tapers sharply. This produces a fast rundown time with the highest maximum axial velocity. Consequently, this design is selected as the reference for construction and use in the 1/4-MJ facility.

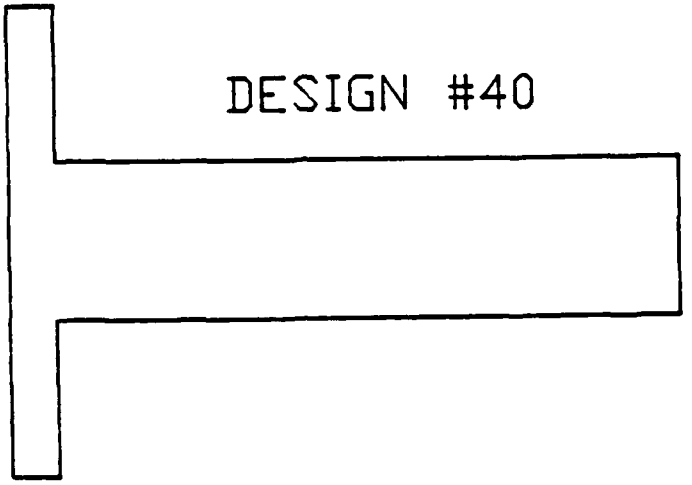

Figure 3

Reference Cylindrical Electrode. The scale in this figure and those following corresponds to an electrode length of 19.6 cm with other dimensions being proportionately scaled.

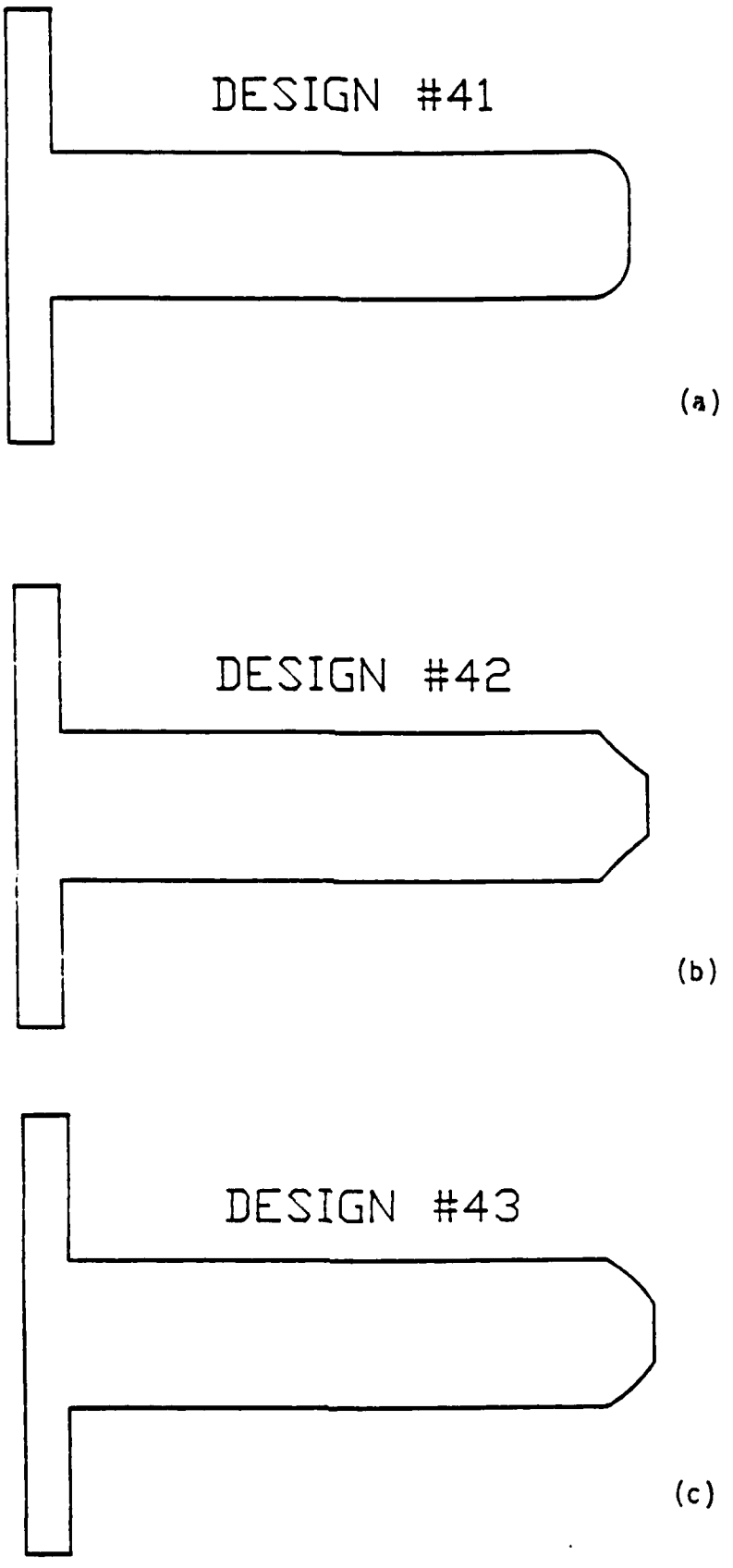

Figure 4

Various Designs with Sculptured Tips. (a) Rounded tip, 1" curvature. (b) Concave tip, 1" curvature. (c) Rounded tip, gradual 1" curvature.

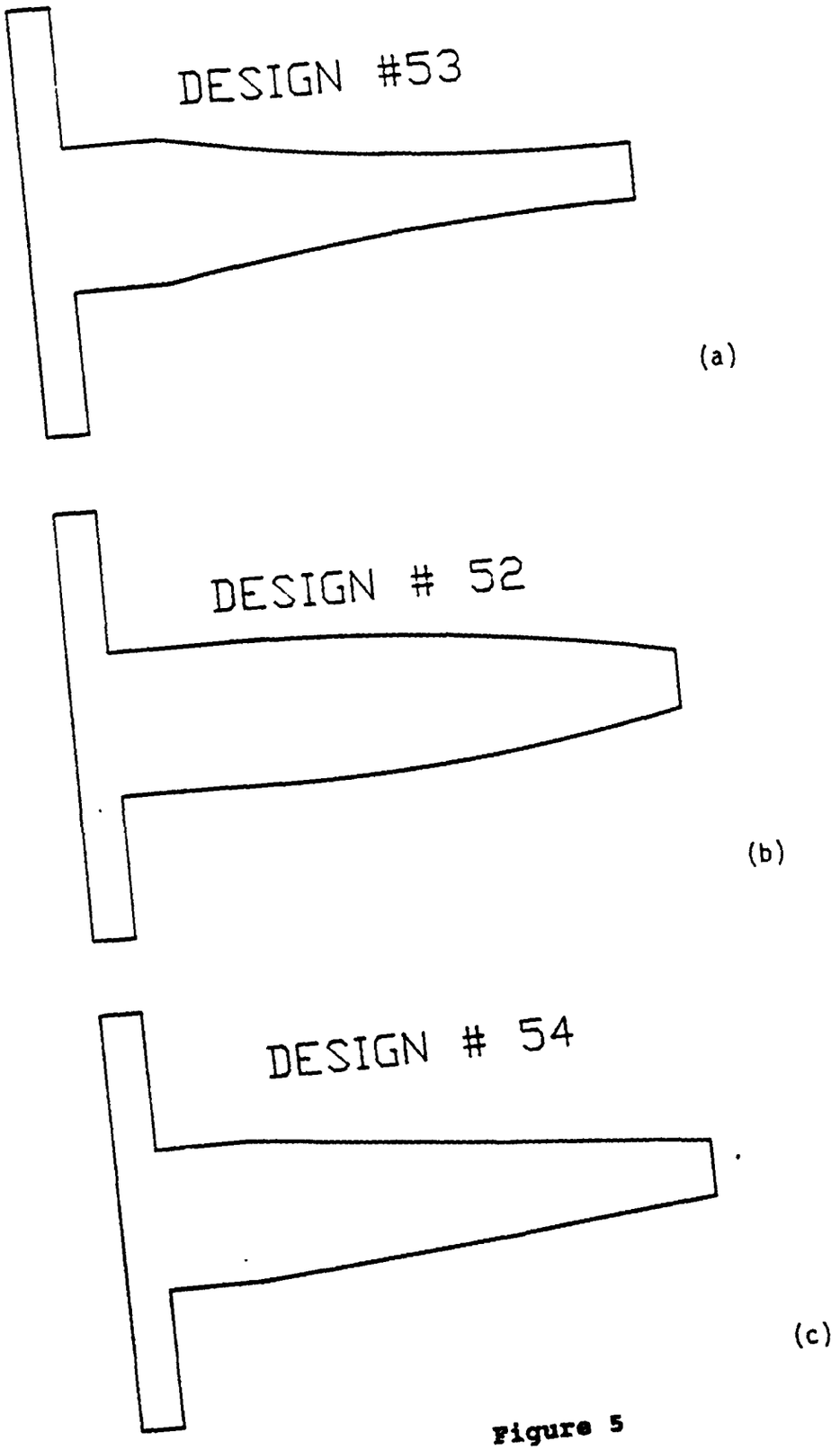

Figure 5

Electrode Designs Employing Various Axial Tapers. (a) Tapered electrode, 12" curvature. (b) Tapered electrode, 12" concave curvature. (c) Tapered electrode, 12" linear taper.

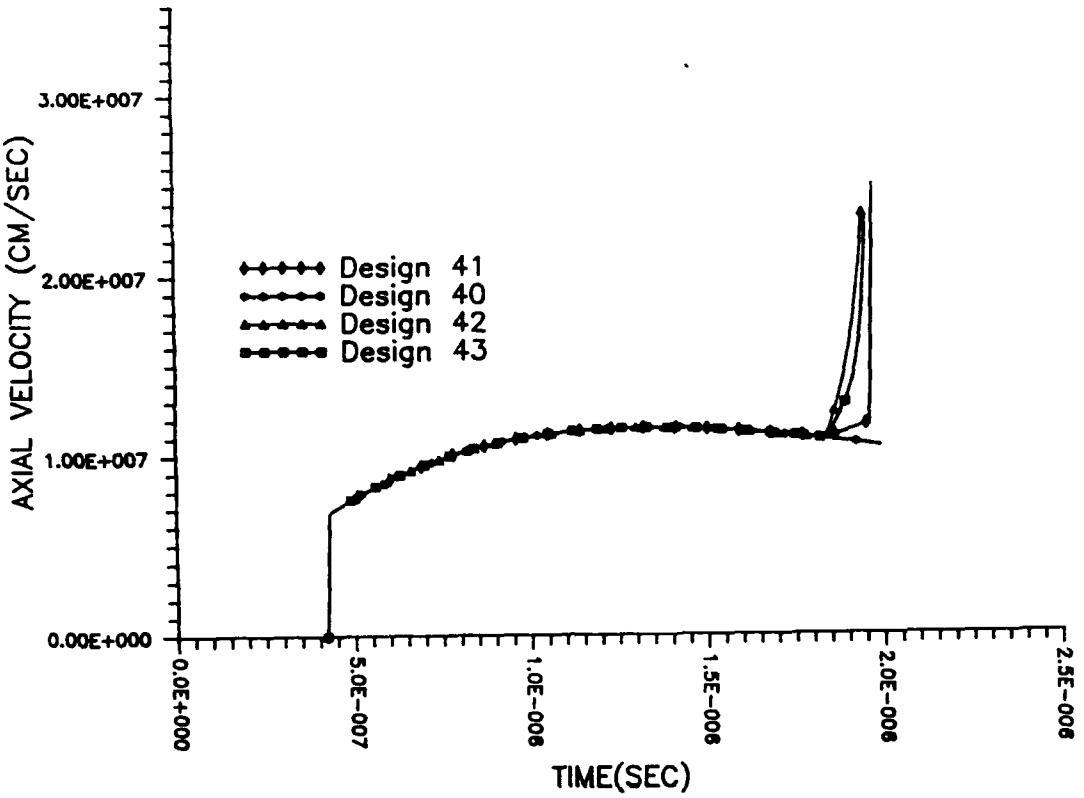

Figure 6

Axial Velocity vs. Time for Electrode Designs 41-44.

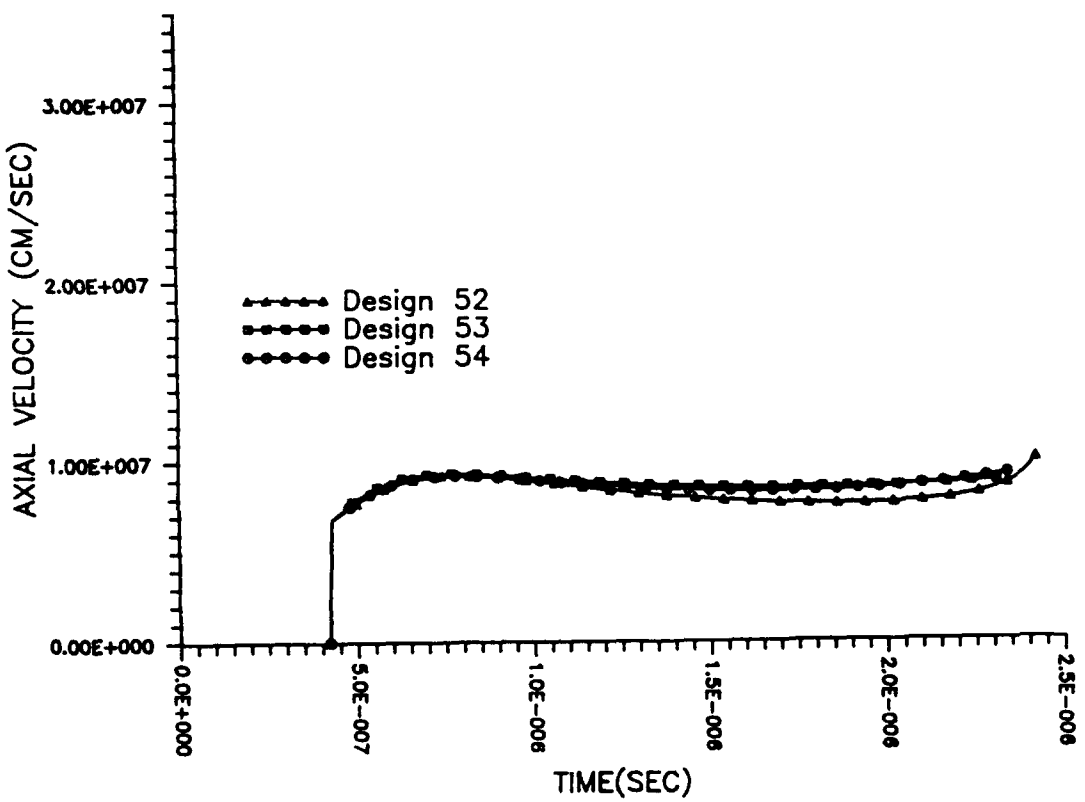

Figure 7

Axial Velocity vs. Time for Electrode Designs 50-54.

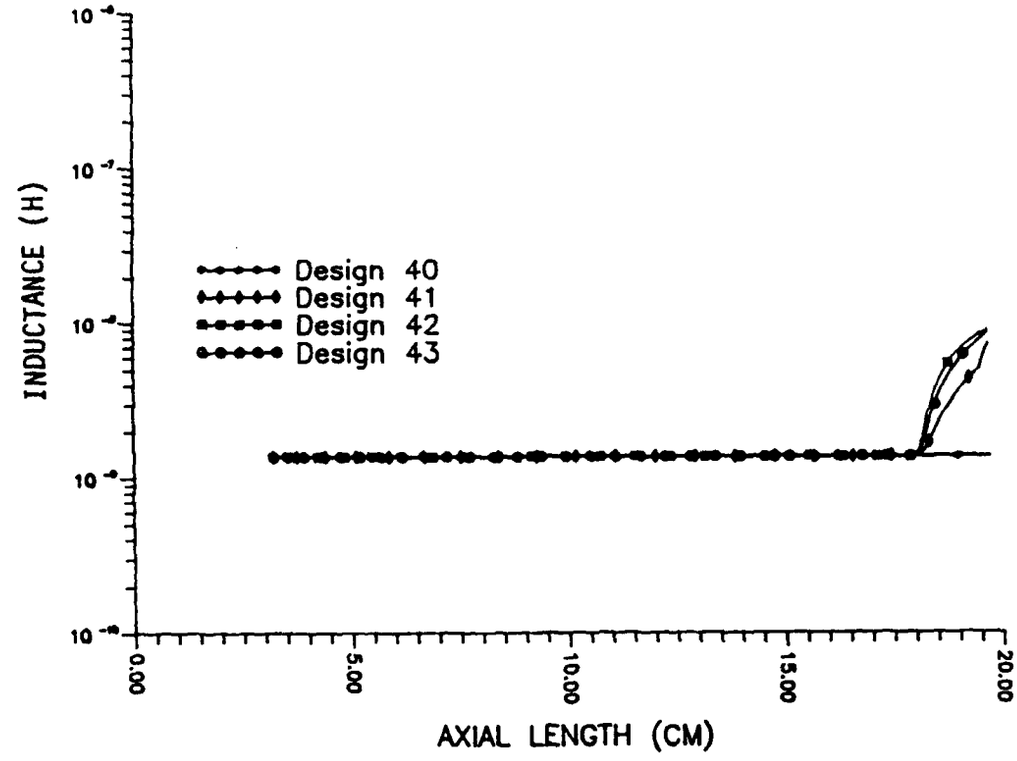

Figure 8

Inductance vs. Length for Electrode Designs 40-43.

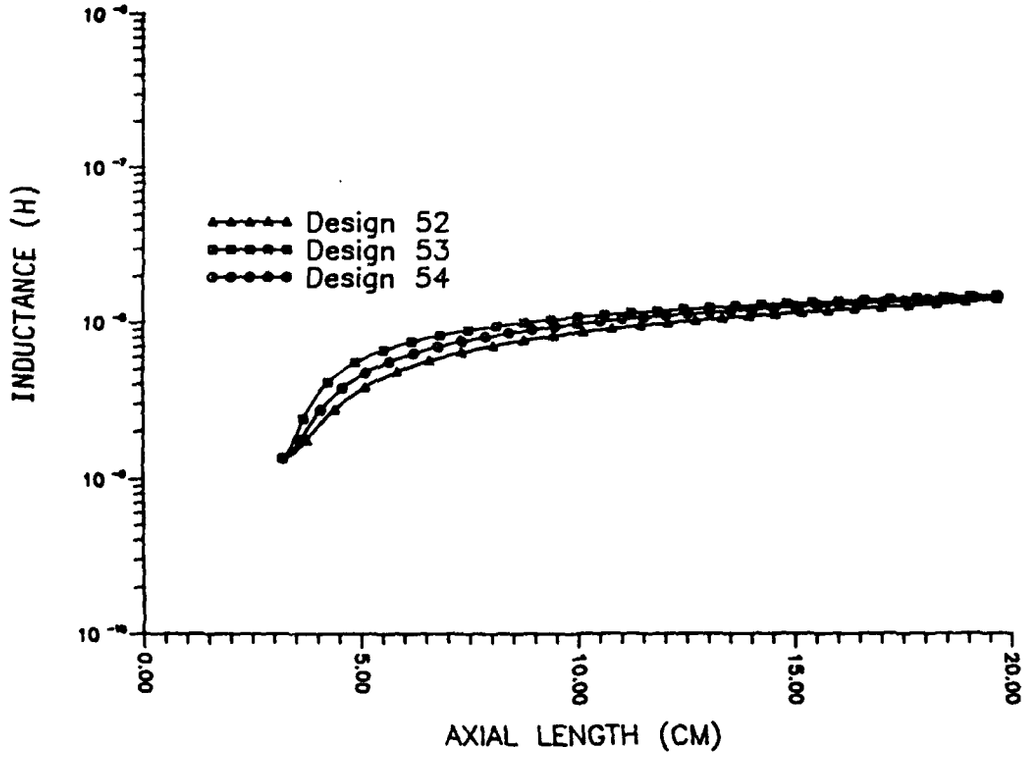

Figure 9

Inductance vs. Length for Electrode Designs 52-54.

Gas Injection System

Introduction. The analysis that we have employed should be quite good for static fill operation of the DPF. However, some adjustments in the design may be found desirable for the gas injected mode. Other studies involving co-axial plasma guns (closely related to the DPF, but without a pinch phase) indicate that optimized gas-injection designs are not too different from static fill operation. However, for the DPF, the pinch phase may bring in some significant differences. The present run-down code does not handle this phase well. Indeed a full 3-dimensional treatment is required to accurately treat the problem theoretically. Thus our approach is to study the reference electrode design selected here with extensive experiments during Phase II. This will allow the run-down code to be normalized to the experimental results if large deviations are found. Also, if necessary, the electrode may be modified in order to further optimize its performance. These results will then be used to design a scaled up version of the electrode system for tests at the 1-MJ level.

One method available to modify the rundown dynamics of the system experimentally is to change the mass injected between the electrodes. Up to a point, increasing the mass between the electrodes can serve to slow down the rundown time, increase the thrust, and possibly increase energy transfer to the load. Thus the gas-injection system (described next) has been designed to accommodate injection rates much higher than calculated here in order to explore a wide parameter range.

The use of a gas injection system is a key element in the development of a DPF thruster of the type proposed by Rockford Technology Associates. Such a system has not previously been employed on a DPF although several prior designs have injected gases at the end or middle of the DPF electrode and at the base of coaxial plasma gun type accelerators. These earlier designs have been carefully considered in the development of the system described here. However, since this is a "first of the kind" unit, Rockford staff have spent considerable effort in its design and in experimentally optimizing its performance.

An illustration of the gas injection system constructed for use with the 10-kJ bank is shown in Fig. 10. The design for the 1/4-MJ unit will, in effect, be a scaled up version of this unit, although some details of the valve will be modified.

The injection system basically consists of a plenum located above the upper conducting plate which is connected to a cylindrical inlet port between the electrodes. The gas flows into the plenum from four gas tubes on the top of the

system which branch out from one gas tube coming from the gas cylinder. Gas flows out of the plenum from the inlet port into the vacuum chamber. Gas is confined in the plenum by a gas valve at the intersection of the four tubes at the top of the system and by a ring valve located between the plenum and the inlet port. The ring valve is opened by four solenoids located above the plenum and is attached to the ring by four rods. Additional pieces are used to compress and seal the system for gas leaks. The entire assembly is azimuthally symmetric around the electrodes.

Azimuthal symmetry is designed in the gas injection system to ensure an azimuthally uniform current flow and gas flow. The plenum, ring valve, and inlet port are constructed so that an azimuthally uniform slug of gas will flow between the electrodes when the ring valve is opened. The ring valve is opened uniformly by placing the lifting rods evenly around the ring valve. The gas tubes are evenly spaced so the plenum fills in an uniform manner. The gas tubes and ring valve lifting rods intersect the base plate of the inner electrode and cause interruptions in the current flow. By having the current interruptions evenly spaced around the electrode the azimuthal symmetry of the current flow is preserved. The use of symmetry in the design makes it unnecessary to perform difficult calculations to account for any asymmetric effects on the gas flow and current flow. The symmetric design of the system also allows the parts to be assembled at any angular orientation.

All of the parts of the gas injection system are designed to be assembled vertically. This is important due to the vertical orientation of the electrodes for Rockford's DPF's. Only a small area inside the diameter of the top compression plate need's to be assembled and disassembled in order to install and service the gas injection system. The vertical assembly requires no special tools or great feats of manual dexterity to assemble. The symmetric design of the system allows the pieces to be layered on top of each other without concern for their azimuthal orientation. Thus as long as the proper sequence of assembly is used, assembly and maintenance of the gas injection system can easily be performed by one person in a short time.

Description of Individual Pieces. Discussion of the individual parts will begin from the bottom of the system and work its way up to the top of the system. Each part described is numbered and can be easily found in Fig. 10.

At the base of the electrodes pieces #1, #2, and #3 fit together to form the inlet port. The inlet port is a cylindrical slit 3/16" wide which directs the gas from the base of the plenum to the base of the electrodes. Many criteria were considered in the inlet port design. The

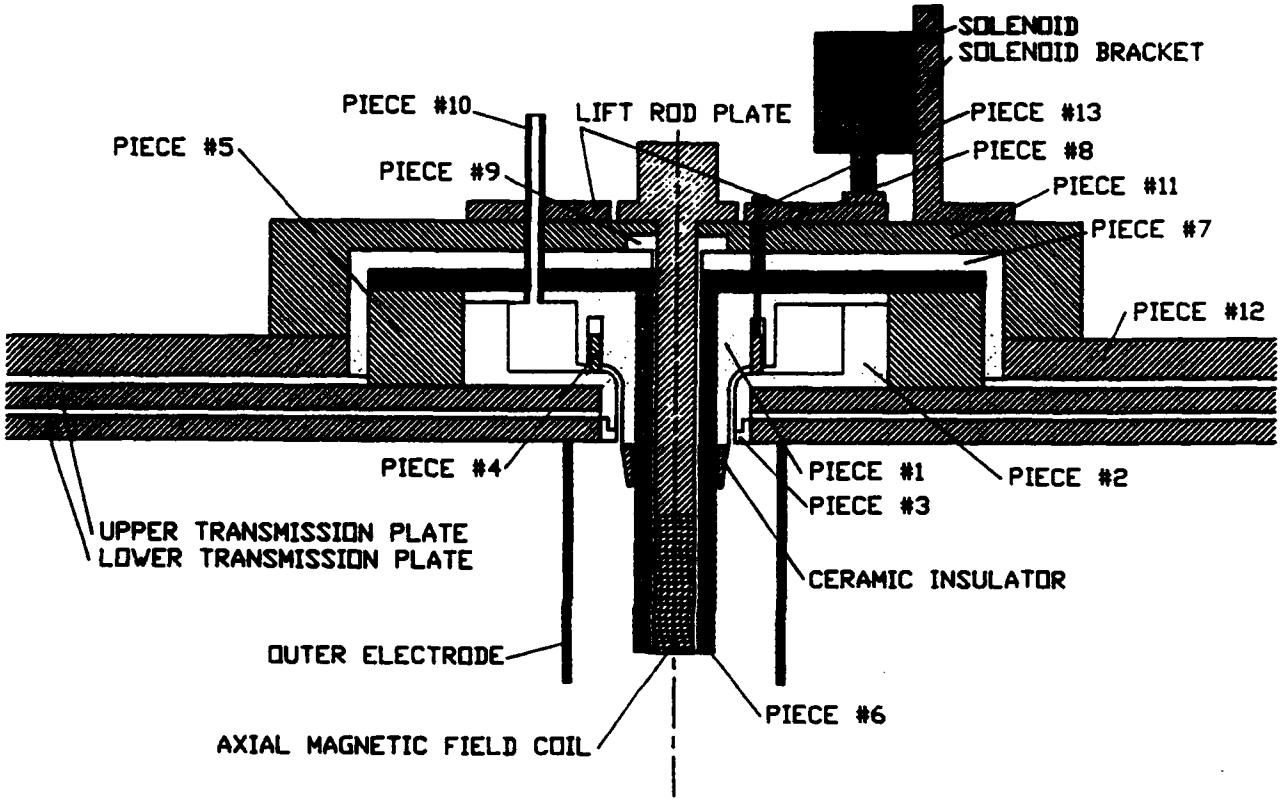

Figure 10

Gas-Injected Plasma Focus.

Piece Number	Item Description
1	Ring valve containment piece
2	Plenum basic piece
3	Transmission plate seal
4	Ring valve ring
5	Aluminum conducting ring
6	Inner electrode
7	Electrode containment piece
8	Lift rod guide tube
9	Axial B-field insulating piece
10	Gas extension tube
11	Aluminum cover plate
12	Aluminum compression plate
13	Lift rod

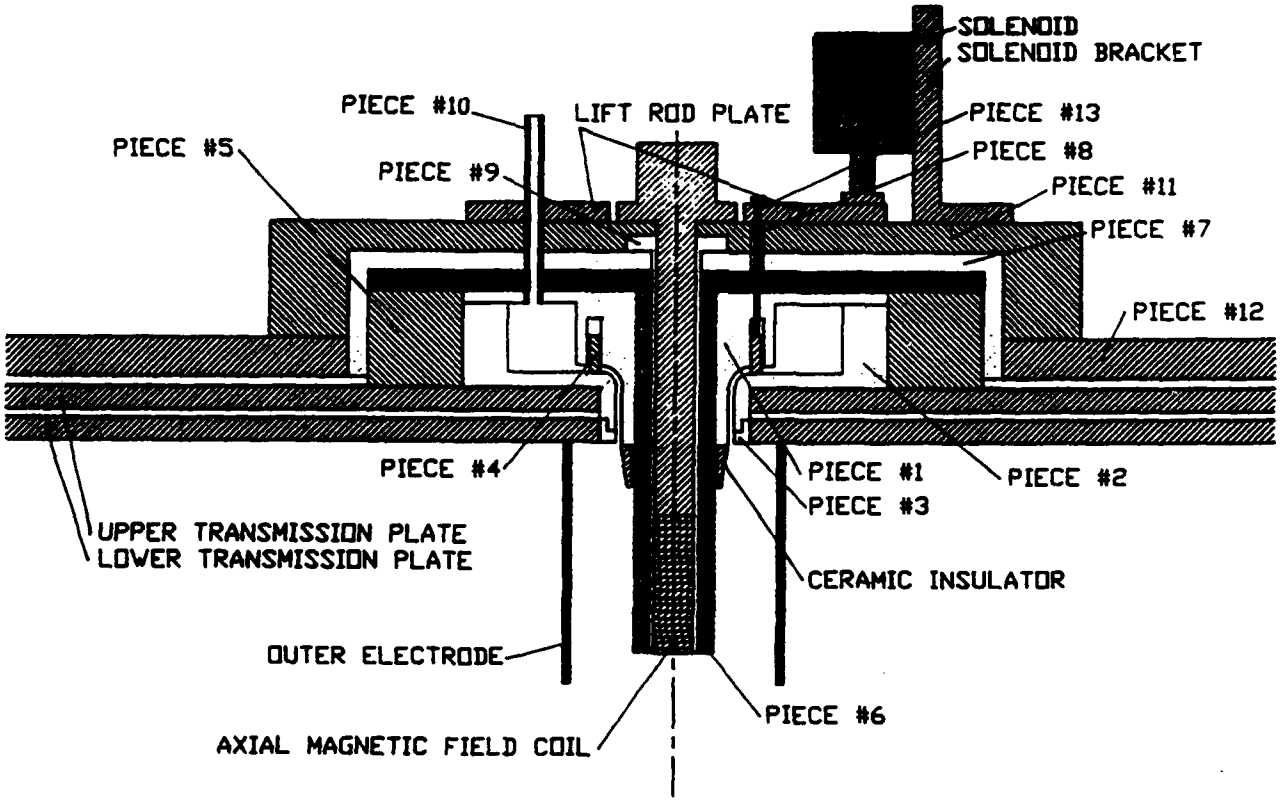

Figure 10

Gas-Injected Plasma Focus.

Piece Number	Item Description
1	Ring valve containment piece
2	Plenum basic piece
3	Transmission plate seal
4	Ring valve ring
5	Aluminum conducting ring
6	Inner electrode
7	Electrode containment piece
8	Lift rod guide tube
9	Axial B-field insulating piece
10	Gas extension tube
11	Aluminum cover plate
12	Aluminum compression plate
13	Lift rod

port increases the chances of arcing between the plates due to the increased exposure to gas. Leakage along the mylar sheets which lie between the two plates as an insulator is seen as a problem. In order to isolate the mylar sheets from the gas flow, the original radius of the mylar sheets was decreased by 3/16" so piece #2 could overlap piece #3 and seal along an O-ring in piece #3. The overlapping of the two pieces also gives a smooth path for the gas flow through the inlet port.

Making pieces #2 and #3 one piece in order to seal off the plates was ruled out even though it would give a better vacuum seal. If the gas injection system did not function well for radiation experiments it would be necessary to place the original parts back into the system in order to carry out different experiments. Making pieces #2 and #3 one piece would require disassembly of the vacuum chamber under the conducting plates in order to reinstall the original system. Keeping the pieces separate allows replacement of the original parts from the top of the focus. Also the separate pieces make it possible to vertically assemble the system from the top. Therefore the installation and replacement of the different systems is kept a one man job which can be performed in a short time.

The inlet port is sealed off from the plenum by the ring valve assembly. The ring valve assembly is composed of a hollow Aluminum disc (piece #4) which rides in a slot machined in the upper part of piece #1. The inlet port is sealed by compression on an O-ring at the base of piece #2 by piece #4. The downward force is exerted by four springs evenly spaced around piece #4. Piece #4, called the ring, is sealed by two O-rings on each side. A pair of O-rings are used on each side of the ring in order to keep the ring as vertical as possible while it is moving up and down in the slot. The O-rings used at the base of piece #2 and on the sides of the ring are Viton O-rings. Viton O-rings require very little vacuum grease to seal along a surface. This is necessary to avoid possible contamination of the ceramic insulator by vacuum grease being carried down through the inlet port by the gas flow. A sleeve (piece #8), cemented to piece #1, guides the lifting rods (piece #13) through the containment pieces and the inner electrode. Piece #8 has additional O-rings around the lifting rods to ensure a vacuum seal and insulate the ring from the inner electrode so any gas which may leak past the ring will not arc from the inner electrode through the inlet port to the outer electrode. The lifting rods are attached to the lift rod plate which is attached to four evenly spaced solenoids. The lift rod plate is needed to attach the lift rods to the solenoids since the solenoids will not fit directly above the lift rods.

The spring and solenoid sizes used on the ring valve assembly had to be experimentally determined. The amount of wall friction exerted by properly sealing O-rings on the ring could not be calculated. Thus the spring force needed to compress the O-ring at the base of piece #2 was found by testing different sizes of springs in the ring valve. Once the spring size was determined the solenoid strength could be found. Original plans had the solenoids placed under the aluminum containment piece. However, initial tests with small solenoids were unsuccessful in lifting the ring up against the force of the springs. Larger solenoids were used to achieve a quick opening ring. With the use of large solenoids it became necessary to move the solenoid outside the aluminum containment piece. The lifting rods (piece #13) had to be thickened and extended to reach the solenoids.

A plenum was placed between the gas lines and the inlet port to allow the gas to reach equilibrium before opening the ring valve. The plenum is sealed off from the inlet port by compression of an O-ring by the ring valve at the base of the plenum. Lifting the ring valve off the O-ring and across the inlet port gap uniformly should give a uniform slug flow of gas into the inlet port from the plenum. The amount of gas injected into the chamber depends upon the size of the plenum and the gas pressure in the plenum. The radial thickness of the plenum is limited by the diameter of the compression plate and the radial thickness of the aluminum conducting ring. The existence of the plenum alters the path of the current flow from the conducting plate to the inner electrode. The current must flow an additional distance proportional to the height and width of the plenum. The additional distance traveled by the current increases the resistance and lowers the efficiency of the system. Thus the plenum height chosen was limited to 3/4 inch in order to keep the increase in resistance small. The volume of the plenum is approximately 22.4 in^3. Since the plenum size is fixed, the amount of gas can be varied by changing the pressure in the plenum. Additional gas can be added to the flow by leaving the gas valve on the incoming gas line open. Thus, all gas from the gas lines and the gas cylinder will drain into the plenum when the ring valve is open.

The gas lines are connected to the plenum by piece #10. Piece #10 is glued onto piece #1 with PVC cement. These tubes insulate the gas flow from the inner electrode. This is necessary so arcing cannot occur from the inner electrode through the plenum and inlet port to the outer electrode. Arcing is also possible from the inner electrode to the aluminum cover plate (piece #11) is the gas is not isolated from the current flow. Piece #10 is symmetrically placed around the electrode between the lifting rods.

Next to the plenum is the aluminum conducting ring (piece #5). Piece #5 allows current flow from the upper conducting plate to reach the inner electrode. The height of the aluminum ring is the same as plenum pieces #1 and #2 to allow for compression of the O-rings of the plenum pieces. The radius of piece #5 was made as large as possible in order to maximize the conducting surface area between the upper conducting plate and the inner electrode. The surface area of contact with the redesigned inner electrode is 33.77 in^2, which is 11.14 in^2 larger than the original contact surface area.

Lying on top of the plenum and piece #5 is the inner electrode (piece #6). The radius of the base plate of the inner electrode was enlarged to 4.683 inches, the same dimension as the outer radius of the aluminum conducting plate. Extension of the base was necessary to maximize the conducting surface area between the electrode and the conducting ring. To maintain the same electrode length exposed beyond the ceramic insulator, the length of the inner electrode was extended by 0.356 inches to compensate for the height of the plenum. The inner and outer radii of the shaft of the inner electrode are unmodified from the original dimensions of 0.625 inches and 1 inch respectively.

The cover plate (piece #7) lies over the inner electrode to seal the vacuum around the aluminum conducting piece and the gas injection components. The bottom of the cover plate lies on top of a rubber gasket which seals the aluminum conducting ring from the aluminum compression plate. O-rings exist on both faces of the cover plate to seal any vacuum leaks or gas leaks from the lifting rod sleeve and the gas connecting tubes (piece #10). The height of the cover plate is made so all O-rings can be compressed to hold vacuum.

Vacuum inside the inner electrode is maintained by piece #9. This piece fits around the solenoid coil used to generate the axial magnetic field in the pinch region and extends to the bottom of the inner electrode. Piece #9 separates the vacuum region from the solenoid and seals the vacuum with O-rings located at the top flange of the piece.

Compression on the cover plate and piece #9 is exerted by the aluminum cover plate (piece #11). The aluminum cover plate maintains its downward force on the components by twelve bolts which screw into the aluminum compression plate (piece #12). Piece #11 has holes evenly placed around the piece to fit the lifting rod sleeves and the gas connecting tubes through. Mounting brackets are placed on top of the aluminum cover plate to secure the solenoids used to lift the ring valve.

Preserving the axial magnetic field coil for the gas-injected experiment required the valve design for the plenum to be restricted to the design given. The design of piece #1 in Fig. 10 requires precise machining of the ring for the ring valve in order to achieve gas containment and vacuum seal. Considerable fine adjustments were performed on the ring in order to achieve a vacuum seal. Constant opening of the valve will require frequent adjustment of the O-rings on the ring valve.

If leakage is too difficult to contain with frequent adjustments, the timing circuit can be utilized to minimize leakage. Tests with the PPT's can be performed to measure the leakage from the system. A rough estimate of the leakage rate can be found in this fashion and used to give an estimate of when the timing circuit should be opened before significant leakage occurs. The plenum can be pressurized to the desired pressure quickly so maintaining plenum pressure is not a problem. Thus the timing circuit would open the gas valve to the plenum at a given time to pressurize the plenum and then open the ring valve at another predetermined time to open the ring valve. Achieving the correct time intervals for the operation of the ring valve will be tedious. However, use of the PPT to obtain gas profiles for the gas injection should make that task easier. Once the basic intervals are found, the operation of the system should be easy to perform consistently.

The components of the gas-injection system are designed to be flexible for various ranges of operation. This flexibility will hopefully allow for optimization of the gas injected system for thrust. Design of the plenum to contain gas pressures far above the amount calculated for equating mass densities for the two modes of operation should enable optimal thrust to be achieved. If leakage of the gas in the plenum becomes a problem at higher plenum pressures, then the ring valve opening time can be decreased through the timing circuit. The ring valve will then serve as a gas flow restrictor rather than as a shut off valve between the plenum and the vacuum chamber. Rundown parameters are sensitive to the mass distribution between the electrodes. The ability to control the mass flow between the electrodes is crucial. Measurement of the gas injection pressure at various locations combined with millisecond precision of the timing circuit should enable the operators of the system to obtain the desired mass flow for optimal thrust.

Advanced Gas Puff Valve. The gas valve and injection system described above have been constructed for 10-kJ DPF experiments. In order to scale it up to the 1/4-MJ unit, several issues have been considered, namely:

- achieving a faster rise time

- reduction of the influence of jitter in the Marx generator
- development of a prototype capable of a high repetition rate as is eventually desired in a practical thruster
- isolation of components from rf surges.

To study this, a computer model of the present system was developed as described in Appendix D. Results from the analysis described there indicate several improvements that will be included in the next unit.

Some slight modifications of the 10-kJ design are proposed for use on the 1/4-MJ DPF facility. These include building a dedicated pulser for the solenoids and using the thyratron/capacitor cabinet for triggering the main spark gaps. However, the gas puff system must undergo a complete redesign for kHz operation using the modification of a scheme developed at Cornell. This system has been studied in some detail as described in Appendix D. Among the changes recommended there is the installation of an optical insulator between the computer controller and the solenoid system to protect against rf-surge-induced damage.

Control System/Timing Circuit

Proper operation of the gas injection requires the sequential opening of the gas valves and firing of the capacitor banks. The time intervals between each event must be consistent in order to properly operate and optimize the performance of the system. The short length of the time intervals require a timing system which can perform each event consistently.

A timing circuit was developed to operate the UI DPF with the new gas injection system. A schematic illustration of the timing circuit is given in Fig. 11. The timing circuit controls three peripheral devices; the Marx generator gas line solenoid which fires the system, the ring valve solenoids, and the electromagnetic switches which allow current flow to the axial magnetic field. Control of the peripheral devices is performed by three basics components of the timing circuit; the relay switches, the interface switches, and the computer.

The relay switches consist of three Crystrom 6402A and two Crystrom 6201A circuits. Each 6402A circuit toggles on and off a 240 volt, 3 amp. AC current from voltage signals received from the computer DAAC board. The 6201A circuit monitors the AC voltage status of a power line and sends

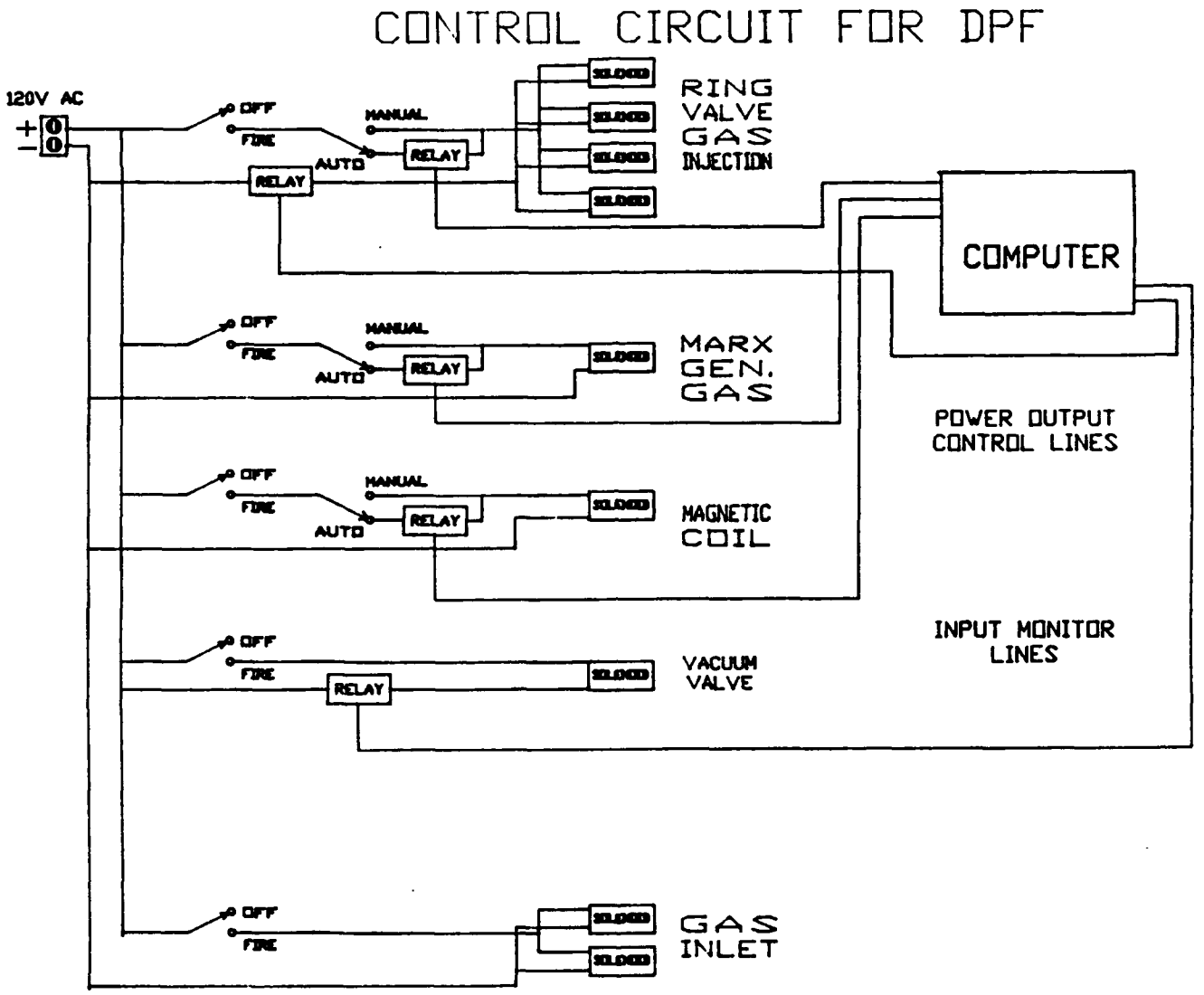

Figure 11

Control Circuit for DPF.

voltage signals to the computer DAAC board. Unlike most relay circuits, a high voltage signal from the computer DAAC board toggles off the 6402A circuit and corresponds to zero voltage on the 6201A circuit. Initially the 6402A circuits must be turned off by the computer when the timing circuit is run.

The interface switches are three manually operated toggle switches which allow manual or automated operation of the ring valve solenoids, axial magnetic coil, and Marx generator. The timing circuit allows automated firing of the focus for both modes of operation. When a switch is toggled in the manual position the corresponding device can be operated manually without involving the relay circuit. Thus if the timing circuit fails, the peripheral devices can still be operated manually.

The computer controlling the relay circuits is an IBM model 5150 personal computer. The relay circuits are interfaced to a DAAC board installed in the computer. A fortran program named NU2 controls the firing sequence of the gas injected system. A safety feature was put in the program which disables the system during each run if the electromagnetic vacuum valve is open or the ring valve solenoids are left on manual control. The program calls for input from the 6201A relay circuits which monitor the AC voltage status of the vacuum valve and the ring valve solenoid power lines. A low voltage signal from the circuits to the DAAC board correlates to an ON power status in the AC lines. As the computer boots up the DAAC board, output signals are all set low which toggles on all of the 6402A circuits. To toggle off the 6402A circuits the program must set all outputs from the DAAC board to the 6402A circuits high at the beginning of the program. All operation of the relay circuits is carried out in the program with the reverse logic described above.

The gas injected mode of operation must be have precise control in order to work properly, and this requirement is well suited to use of a computerized control scheme. The pressurized chamber mode of operation can be run manually or controlled by the computer. Thus each peripheral device is wired in parallel to the relay switches and the interface switches. Each interface switch is wired in series with a manually operated on/off switch. For computer operation of the focus each interface switch is set to automatic and its corresponding manual switch is set on. Power to the peripheral devices is toggled on and off by the relay circuits. For manual operation the interface switches are set to manual and power to the peripheral devices is toggled on and off by the corresponding manual switch. At present only the devices related to the fire control of the system have been automated. However the entire focus can be easily

automated by installing additional relay circuits, interface switches, and expanding the program.

The determination of the time intervals for the timing circuit must be performed experimentally. The time intervals can be measured from sets of dual voltage measurements of the trigger signals from the computer to the relay circuits on a storage oscilloscope. The important events to be measured are the trigger signal to the Marx generator relay circuit and the discharging of the capacitor banks; the trigger signal to the ring valve solenoid relay circuits and the trigger signal to the Marx generator; and the trigger signal from the ring valve solenoid relay circuit and a piezoelectric pressure transducer (PPT) set at the breech of the gas-injection system.

A Rogowski coil exists on the transmission plate to the electrodes. The Rogowski coil measures the change of current with respect to time and outputs a voltage signal from this. The voltage output from the coil can be stored on the storage oscilloscope along with the voltage trigger signal from the computer to the relay circuit. The time interval between the events can be measured from the stored image and used to set the approximate interval for the timing circuit program.

Similar measurements can be performed on the time intervals for the opening of the ring valve. A piezoelectric pressure transducer can be installed at the breech of the gas-injection system to measure the pressure of the gas flow into the plenum. The pressure is calibrated in terms of voltage which can be measured on an oscilloscope. The critical pressure for the initiation of the arc can be found from the Pashen curve. However, the pressure at which the system may be triggered will probably be higher than the critical pressure due to the desire to inject larger amounts of gas for propulsion purposes. The desired voltage corresponding to this pressure will be stored on the oscilloscope along with the voltage signal from the relay circuit. The interval between events can be determined from the oscilloscope image.

The easiest measurement will be the time interval between the trigger signal to the ring valve relay circuit and the trigger signal to the Marx generator relay circuit. Both signals can easily captured by attaching voltage probes to the circuit board.

Once all of these intervals have been determined, the time values can be used as starting points in experimentally finding time intervals for optimal performance of the system.

Basic testing of the timing circuit can be performed by operating components of the DPF with the timing circuit. Random time intervals can be inserted into the code and operation of the corresponding components observed. The program NU2 was used to run the Marx generator, axial magnetic field, and ring valve in their proper time sequence. All test runs made were successful.

The success of random time interval test runs on the timing circuit show the basic design to be generally trouble free. One limitation of the system is that the smallest time increment for the time intervals is one millisecond. This time limit originates in the IBM 5150 computer. If this becomes a problem, the replacement of a circuit board in the computer with a board with faster chips would decrease the time increment. Since the program can be used on any IBM compatible computer, installing it on a faster computer is also an option. The fortran code used in this system is described in Appendix B.

Advanced Target Design Concept

As stressed earlier, a major advantage of the DPF thruster is that significant additional energy is gained from charged fusion products generated by fusion reactions during the pinch phase. However, the low $n\tau$ product of gaseous DPF (10^{12}sec/cm^3) rules out any thermonuclear burn following the m = 0 instability produced hot ions. Thus the present study was undertaken to find ways to further increase the fusion gain by imploding a dense gas pinch or frozen fiber failed following cold core at peak compression. Thus, while normal DPF pinch operation is attractive, we have sought innovative ways to further improve this concept. As a result of this effort, we have developed an alternative scheme to implode a magnetically stabilized DPF on a hollow foamed fusionable target placed at the focal line of the DPF electrodes. The proposed scheme appears to have some advantages over the frozen fiber approach. These include: significant stabilization due to axial magnetic field penetration into the target before peak compression, and spark ignition from instabilities promoted by prefabricated grooves on the target wall.

Preliminary calculations were done as described in Appendix C using a modified 0-D MHD code. Results indicate that it is possible to achieve a 0.8-keV plasma with a 10/1 length/diameter ratio and confinement parameter $n\tau$ ~8×10^{12}sec/cm^3 using a 100-kJ DPF imploded on a 1-mg hollow, foamed target driven by a 900 kJ capacitor bank. In contrast, depositing 1 MJ into a 30 torr magnetically stabilized deuterium would result in 1.5-keV core with a length/diameter ratio < 1 and $n\tau = 5\times10^{12}$sec/cm^3.

This target can be tested with Rockford's proposed 1-MJ DPF facility. Preliminary tests of the "spark ignition" scheme could be carried out on the 1/4-MJ module using various thin walled plastic targets with different groove geometries, with and without stabilizing magnetic fields. Advanced diagnostics like a pinhole array covered with spectral resolving X-ray filter array could be used to evaluate the hot ion production efficiency.

Facility Design: 1/4- & 1-MJ DPF

Before constructing the full 1-MJ Dense Plasma Focus (DPF), a 1/4-MJ bank will be constructed and operated first. Construction of a modular facility based on this design is the proposed goal for the Phase II project. Maxwell Laboratories has been selected as the subcontractor to provide for the design and construction of the Pulsed Power Supply (PPS). This includes everything up to the vacuum chamber that will house the DPF (or any other experiment that is contracted to use the PPS). The capacitors for the PPS will not be furnished by Maxwell; instead the University of Illinois (UI) will loan 300 capacitors to Rockford Technology Associates for use in this facility. These capacitors are U. S. DOE property obtained by transfer from the Los Alamos National Laboratory (LANL). The equivalent cost of this capacitor bank, if purchased new, would be ~$2M. Thus use of the former LANL bank is very cost effective.

Capacitors. The specifics of the LANL capacitors are given in Table 1. These are brand new, never before used, capacitors. Their total capacitance exceeds 1-MJ, thus allowing for replacement units should thus be necessary, e.g., due to capacitor failure during operation.

Table 1. 1-MJ Facility Capacitor Parameters

Manufacturer:	Aerovox
Model Number:	PX300-D51A
Voltage:	60 kV
Capacitance:	2 microFarad
Inductance:	< 70 nH
Weight:	290 lbs/ea.
Dimensions:	25"x14"x11"

Facility. As mentioned above, the 1/4-MJ PPS will be built first; the remaining 1-MJ PPS would then be completed during Phase III. Figure 12 depicts the 1-MJ PPS. The 1-MJ PPS is composed of four quarters. In order to assemble a

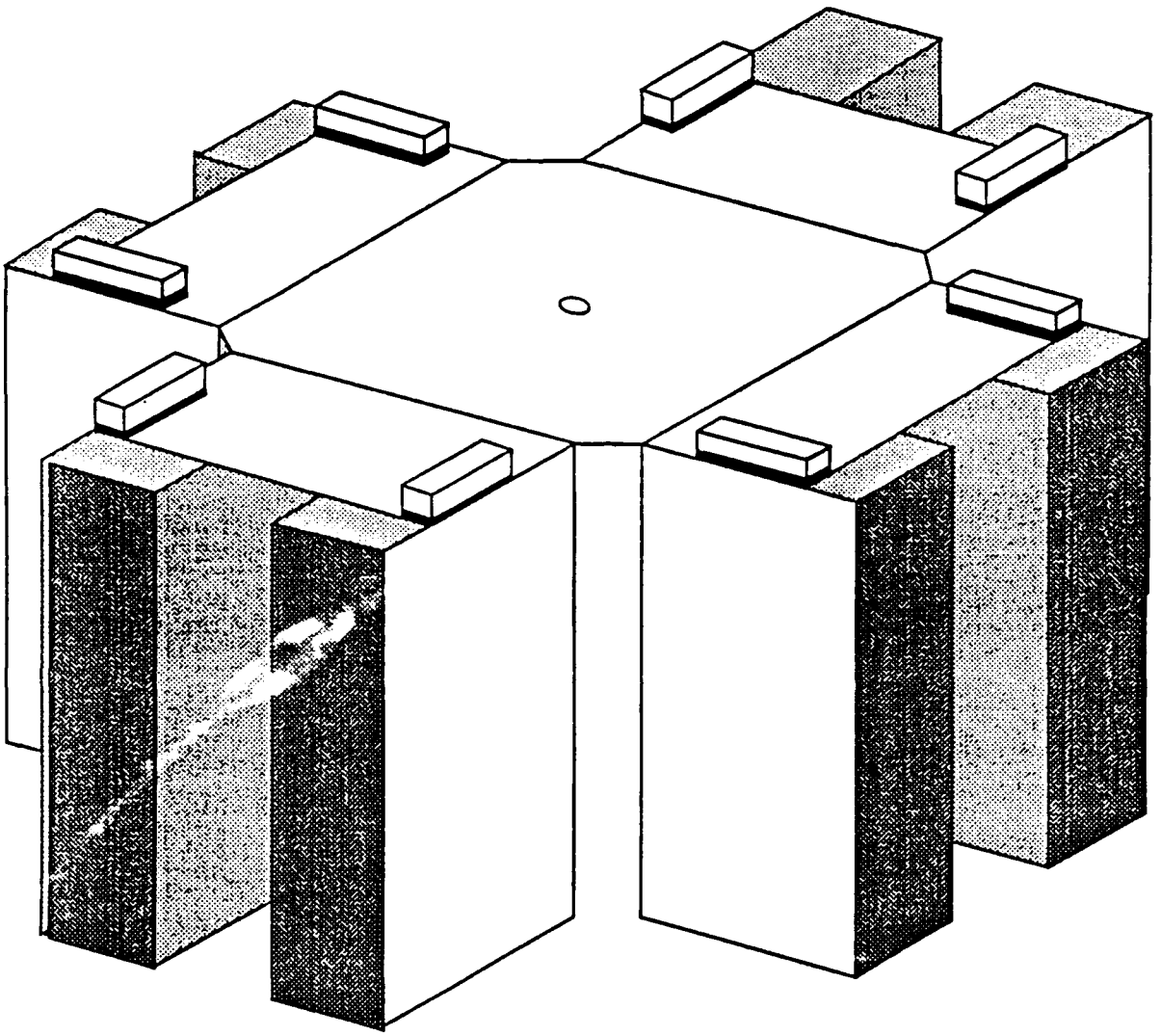

Figure 12

Layout of 1 MJ system.

1/4-MJ facility, the first quarter of the full unit will be constructed first. The modular design of the system will allow for easy addition of the remaining three quarters after the 1/4-MJ tests are complete.

Cost Estimate. Maxwell Laboratories estimates a cost of about $216,000 for construction of the 1/4-MJ PPS. This includes all the hardware needed (minus the capacitors) to assemble one complete 1/4-MJ arm. It does not include the high voltage power supply, power supply controller, nor the trigger generators or gas controllers. However, it does include the control console.

Maxwell has supplied a current price quote for the items not included in the price quote. (Table 2)

Table 2. Price Quotes For Added Equipment

Item	Qty.	Unit Price	Total
Power Supply & Controller	1	$35,000	$35,000
Rail Gap Switch	2	5,790	11,580
Dual Gas Controller	2	1,124	2,248
Trigger Generator	1	9,660	9,660
Trigger Amplifier	1	8,000	8,000
Sum Total			$66,488

Summary

In summary, the Phase I work on this project has met all of the basic objectives. A modular design has been developed for the construction of a 1-MJ plasma focus facility which is capable of obtaining vital scaling information for the development of plasma focus type MPD thrusters. It is viewed that the experimental work using this facility would ultimately provide the database necessary to continue studies of a prototype thruster at higher energies. For that purpose preliminary contact has been made with Air Force scientists at the Phillips Laboratory where use of the 9-MJ pulse power facility there is ultimately contemplated.

References

1 Decker, G., Herold, H., Kaeppeler, H.J., Kies, W., Maysenhölder, W., Nahrath, B., Oppenländer, T., Pross,G., Rückle, B., Sauerbrunn, A., Schilling, P., Schmidt, H., Shakhatre, M., and Trunk, M., "Neutron Emission Parameters In Plasma Focus Devices," Plasma Physics and Controlled Nuclear Fusion Research Conference Proceedings, Vienna 1978), Vol. 2, International Atomic Energy Agency, Vienna, 1979, pp. 135-142.

2 Maxon, Stephen, "Two-Dimensional MHD Calculations for a 5MJ Plasma Focus," Energy Storage, Compression and Switching, ed. by Nardi, V., Sahlin, H., and Bostick, W.H., Vol. 2, pp. 387-405, 1978.

3 Potter, D.E., "Numerical Studies of the Plasma Focus," Physics of Fluids. Vol. 14 (9) Sep 1971, American Institute of Physics, pp. 1911-1924.

4 Kondoh, Y., and Hirano, K., "Numerical Study of an Ion Acceleration in a Z-pinch Type Plasma Focus," Physics of Fluids. Vol. 21 (9) Sep 1978, American Institute of Physics, pp. 1617-1622.

5 Gourlan, Corantin, Kroegler, Horst, Maisonni, Charles, Rager, Jean Pierre, and Robouch, Benjamin V., "Present Status of the Frascati 1MJ Plasma Focus Programme," Energy Storage, Compression and Switching, ed. by Nardi, V., Sahlin, H., and Bostic, W.H., Vol. 2, pp 221-245.

6 Mather, J.W., "Dense Plasma Focus," Methods of Experimental Physics, Ed. Lovberg, Ralph H., and Griem, Hans R., New York: Academic Press, 1971, pp. 187-249.

7 Herold, H., Jerzykiewicz, A., Sadowski, M., and Schmidt, H., "Comparative Analysis of Large Plasma Focus Experiments Performed at IPF, Stuttgart, and at IPF, Swierk," Nuclear Fusion. Vol. 29, No. 8 (1989), International Atomic Energy Agency, pp. 1255-1269.

8 Gates, "Studies of a 60 kV Plasma Focus," Energy Storage, Compression and Switching, ed. by Nardi, V., Sahlin, H., and Bostick, W.H., Vol. 2., pp.329-351.

9 Mandrekas, J., "Zero-Dimensional Model for the Dense Plasma Focus," Master of Science Thesis, Department of Nuclear Engineering, University of Illinois, (1984).

10 Elgroth, Peter G., "Comparison of Plasma Focus Calculations", Phys. Fluids, 25(12), Dec. 1982, pp.2408-2414.

Publications From Phase I Work

Articles:

O. Barnouin, B. Temple, and G. H. Miley, "Plasma Focus Device for Use in Space Propulsion," Fusion Tech., 19, 846-851, 1991.

R. Nachtrieb, O. Barnouin, B. Temple, G. Miley, C. Leakeas, C. Choi, and F. Mead, "Computer Model for Space Propulsion Using Dense Plasma Focus," 18th IEEE Intern. Conf. on Plasma Science, p. 155, Williamsburg, VA, June 3-5, 1991.

O. Barnouin, B. Temple, and G. H. Miley, "Use of a Dense Plasma Focus as an X-ray Irradiation Facility," IEEE Intern. Conf. on Plasma Science, 4P2-13, 190, Oakland, CA, May 21-23, 1990.

G. Miley, R. Nachtrieb, and J. Nadler, "Use of a Plasma Focus Device for Space Propulsion," AIAA/NASA/OAI Conference on Advanced SEI Technologies (AIAA-91-3617), Cleveland, OH, September 4-6, 1991.

Conference Presentations:

G. H. Miley, B. Temple, and J. Nadler, "Magnetic Field Stabilization of Plasma Focus for Thrust Production," Progress and Applications of Plasma Focus Research, Hoboken, NJ, May 27-31, 1991.

G. H. Miley, J. Nadler, and B. Temple, "Review of Plasma Focus Research at the University of Illinois for Space Propulsion," Plasma Focus Propulsion Workshop, Purdue University, May 7-8, 1991.

Reports:

H. Kislev and G. Miley, "Fusionable Propellent for Dense Plasma Focus Thrusters," Project Report RTA-PF-01, Champaign, IL, 30 July 1991.

H. Kislev and G. Miley, "A Repetitive MA Plasma Switch for Dense Plasma Focus Thrusters," Project Report RTA-PF-02, Champaign, IL, 30 July 1991.

H. Kislev and G. Miley, "Gas Puff Valve for Dense Plasma Focus Thruster," Project Report RTA-PF-03, Champaign, IL, 30 July 1991.

APPENDICES

Appendix A

Estimation of Propulsion Exhancement by Fusion Energy Addition in the DPF

Appendix A
Estimate of Propulsion Enhancement by Fusion Energy Addition

The applicability of the Dense Plasma Focus (DPF) to space propulsion is examined for a scaled device, and the contribution of fusion energy to thrust and specific impulse is estimated.

The DPF model consists of two parts: rundown and pinch. During the rundown phase, the gas between the electrodes is ionized and a fraction swept forward (rundown mass) by the current sheath. The electrode lengths are set such that when the current sheath reaches the end, the current delivered by the capacitor banks is at a maximum. (If the current does not reach an absolute maximum during the rundown, the electrode length is set such that the current at the end is an arbitrary fraction of the local maximum current, say 80%.) A fraction of the rundown plasma is then trapped in the pinch phase, while the remainder is exhausted axially.

In the pinch phase, the trapped plasma is constricted by the magnetic field field of the current at the end of the electrodes (maximum). The compressed plasma is heated like an ideal gas to fusion temperatures, with a Maxwellian energy distribution assumed. Fusion reactions occur at a rate corresponding to the density and temperature of the fuel plasma, with the accompanying energy release going to heat the rocket propellant.

During the rundown phase, the DPF is approximated by an RLC circuit, depicted in Fig. A-1, with the inductance increasing at a constant rate[1].

The time rate of change of the inductance, $\dot{L}$, is proportional to the plasma rundown velocity, experimentally determined to be roughly constant.

$$\dot{L} = v_{run} \frac{\mu_0}{2\pi} \ln\left(\frac{r_c}{r_a}\right)$$

where r_c and r_a are the cathode and anode radii, respectively.

Solving for the charge on the capacitor as a function of time, $q(t)$, yields a series solution

$$q(t) = \sum_{n=0}^{\infty} A_n t^n$$

$$A_0 = \frac{1}{U_0} 2W$$

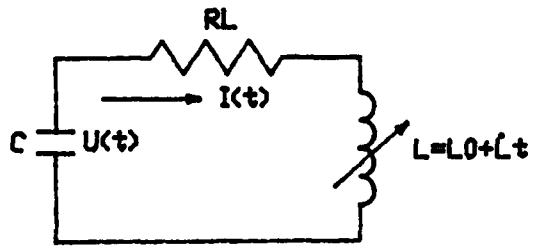

Figure A-1
DPF Rundown Circuit

$$
\begin{aligned}
A_1 &= 0 \\
A_2 &= -\frac{\dot{I}_0}{2} \\
A_{n+2} &= -A_n \frac{U_0 \dot{I}_0}{2W} \frac{1}{(n+1)(n+2)} \\
&\quad -A_{n+1}(R_l + \dot{L}(n+1)) \frac{\dot{I}_0}{U_0} \frac{1}{(n+2)}
\end{aligned}
$$

where W, the capacitor bank energy, $\dot{I}_0$, the initial rate of current change, and $\dot{L}$ are held constant. This solution is a polynomial in t; the recursion relation for coefficients A_3 and above is also given.

The voltage on the capacitors is proportional to the charge, and the current delivered as a function of time is simply the negative time derivative of the capacitor charge.

$$
\begin{aligned}
U(t) &= \frac{1}{C} q(t) = \frac{U_0^2}{2W} q(t) \\
I(t) &= -\frac{d}{dt} q(t)
\end{aligned}
$$

The impedance of the plasma focus rises sharply when the pinch begins. This model assumes a jump in the pinch inductance and resistance at the beginning of the pinch, but that the pinch impedance remains constant during the stable pinch lifetime. Fig. A-2 shows the equivalent circuit for the DPF during the pinch phase. The solutions are for a RLC circuit.

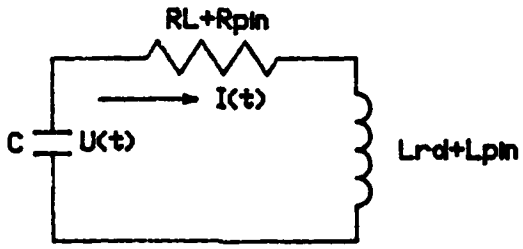

Figure A-2
DPF Pinch Circuit

The pinch is approximated by a cylindrical plasma, whose dimensions remain constant during the stable pinch lifetime. To maintain plasma pinch dimensions, magnetic pressure at the plasma edge must balance the kinetic pressure of the plasma.

$$\frac{\mu_0 I^2}{8\pi^2 r_p^2} = nkT$$

where r_p is the pinch radius, $n = n_i + n_e$ is the particle number density in the pinch, and kT is the particle energy. The pinch becomes unstable when current is no longer delivered from the capacitors ($U = 0$), and thus the magnetic field drops to zero.

The fill gas density is set to provide the maximum reaction rate for the maximum current delivered to the pinch. If one treats the pressure in the pinch as fixed by the induced magnetic field from the maximum current, then there exists plasma temperature for which the reaction rate is a maximum. In the plasma, the reaction rate is proportional to the square of the fuel density and the reaction rate parameter, $<\sigma v>$. The reaction rate is maximized when $<\sigma v> /(kT)^2$ is maximized. For D-3He, this occurs at $kT \approx 47$ keV.

Shown in Figs. A-3 and A-4 are the relative voltage and current profiles as a function of time during the rundown and pinch phases for bank energies of 250 kJ and 100 MJ. Note that for the 250 kJ case, the voltage and current profiles follow expected trends. For the 100 MJ case, the pinch lifetime is very short, so the steady decrease in current occurs very quickly (not shown

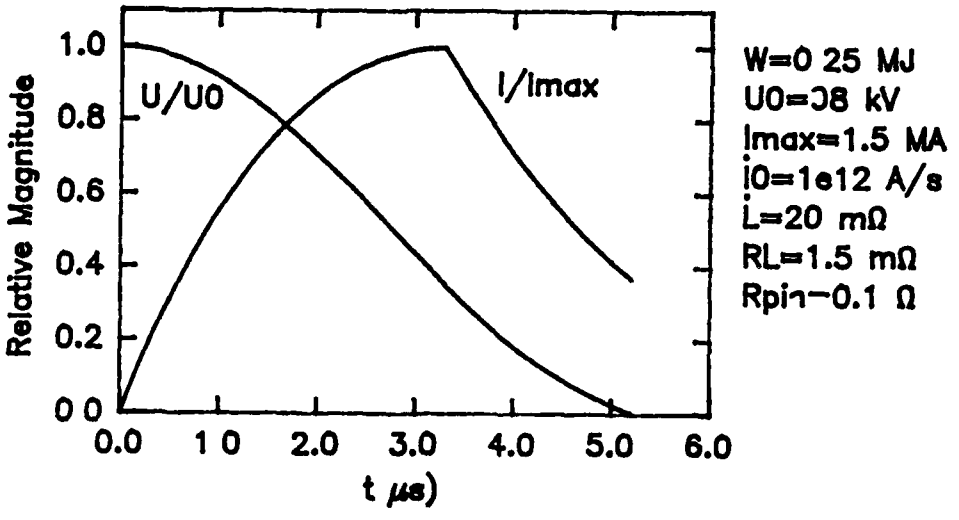

Figure A-3
DPF Voltage and Current Profiles, 250 kJ

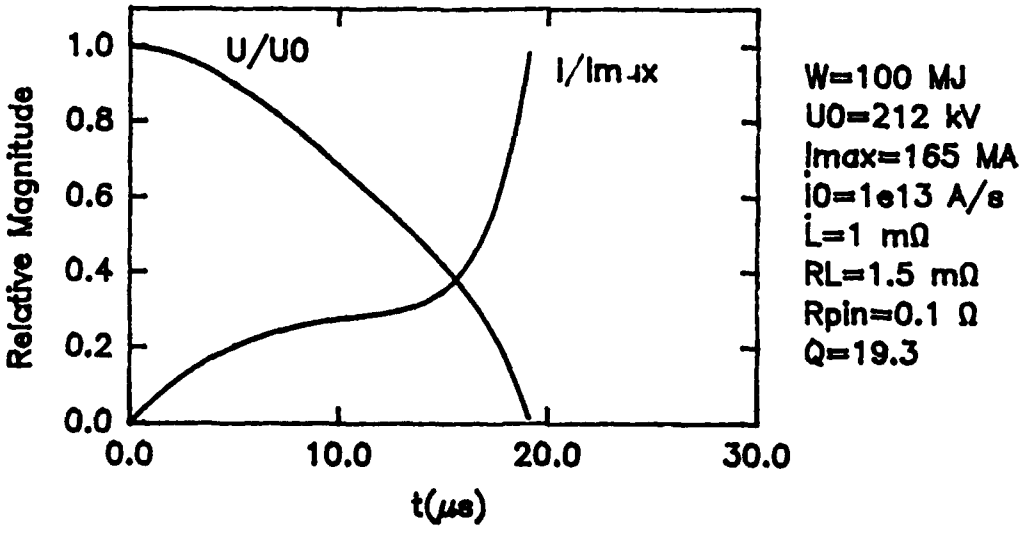

Figure A-4
DPF Voltage and Current Profiles, 100 MJ

Table A-1. Fusion Contribution for Different Bank Energies

Bank Energy (MJ)	0.25	1	10	100
U_0 (kV)	98	156	98	212
$\dot{L}$ (mΩ)	20	20	1	1
$I_{\max}$ (MA)	1.5	2.3	77	165
E_f (MJ)	9.7J	96J	9.3	1830
Q	1	1	1.9	19.3

on graph).

The fusion energy produced during one pulse, E_f, is the integral of the instantaneous fusion power over the pinch lifetime. The total energy out per pulse is the sum of the bank energy, W, and the integrated fusion power, E_f. We can define the gain Q as the total energy out over the input energy.

$$Q \equiv \frac{E_f + W}{W}$$

Table A-1. shows Q values, and other data, from some some cases run. $R_L = 1.5$ mΩ, $R_{pin} = 0.1$ Ω.

The fusion contribution to rocket performance is determined by comparision of thrust and specific impulse (or jet power) when the fill gas is a fusion fuel (deuterium, helium-3) versus when it is inert (hydrogen, helium-4). If one assumes that the majority of the energy from the pinch (all in charged particles) can be converted to useful thrust, then the DPF at higher bank energies looks promising indeed. The ratio of rocket performance with and without fusion contribution, is equal to the ratio of energy output, with and without fusion fuel. This is simply the Q factor.

When compared to otherelectric propulsion devices, which neither use fusion fuels nor provideany energy multiplication whatsoever, the Dense Plasma Focus appears tobe an excellent candidate for space propulsion.

References

[1] Decker, G., et. al, "Neutron Emission Parameters in Plasma Focus Devices," Plasma Physics and Controlled Nuclear Fusion Research Conference Proceedings, Vienna 1978, Vol. 2, IAEA, pp. 136-142

APPENDIX B

Modified Run-Down Code

APPENDIX B

Modified Run-Down Code

The circuit equations for the UI DPF are derived from the circuit drawing in Fig.(2). The equations are as follows:

$$(R_e + R_f)I + L_e\frac{dI}{dt} + L_f\frac{dI}{dt} + I\frac{dL_f}{dt} = V_c \tag{1B}$$

and

$$\frac{dV_c}{dt} = -\frac{I}{C} \tag{2B}$$

Where

R_e = Resistance of the focus assembly

R_f = Resistance of the load (electrodes and plasma)

I = Current

L_e = Inductance of the focus

L_f = Inductance of the electrodes

V_c = Capacitor voltage

C = Capacitance

The circuit equations for the system are valid for all modes of operation.

The inductance for the focus is calculated from the following equations:
For the lift-off phase:

$$L_{le} = \frac{\mu_0 Z_0}{2\pi}\ln\left(\frac{R_{ah}}{R_{in}}\right) \tag{3B}$$

For the rundown phase:

$$L_{rd} = \frac{\mu_0 Z}{2\pi}\ln\left(\frac{R_{out}}{R_{in}}\right) \tag{4B}$$

Where:

Z_0 = Height of the insulator

R_{sh} = Radius of the sheath

Z = Height of the arc rundown

R_{out} = Radius of the outer electrode

These equations assume that the plasma resistance is small compared to the system resistance and dL_f/dt is zero. The lift-off inductance is not considered in the empirical equation for the maximum current and for electrode modifications beyond the height of the insulator. Thus only the rundown inductance is of concern.

The circuit equation is coupled to the equation of motion for the current sheath. In the the rundown phase the acceleration of the current sheath is assumed to be negligible.[23] The pressure balance between the magnetic pressure and the rate of momentum gain per unit area define the equation of motion for the current sheath, given as:

$$\frac{B^2}{2\mu_0} = \rho V^2 \tag{5B}$$

Where:

$$B_\theta = \frac{\mu_0 I}{2\pi R_{sh}} \tag{6B}$$

Equation (5B) holds only for a DPF operated in the static fill mode.

Modifications were made to Mandrekas's code[9] to account for the effects from the change in inner electrode geometry. The code was rewritten with the lift-off and rundown calculations being performed in the subroutines Lift and Rundown instead of being solved in the main body of the code. However, the circuit equation is still solved by a fourth order Runge-Kutta method in the main body of the program. The Rundown subroutine had to be modified to include effects from the inner electrode radius change. Also an additional subroutine named Cramer was added to Mandrekas's rundown code to calculate the various electrode geometries desired.

The subroutine Cramer is used to give a quadratic curve fit to the numbers entered at the start of the program. Initially the program asks for the input of numbers which

relate to three points that describe the radial surface of the inner electrode. The values are checked to ensure the numbers given correlate to the correct range of possible values. Subroutine Cramer sets up a series of three quadratic equations where the radius of the electrode R is the independent varible and the axial position Z is the dependent varible. For a set of three points (R_1,Z_1), (R_2,Z_2), and (R_3,Z_3), the system of equations are:

$$AR_1^2 + BR_1 + C = Z_1 \qquad (7BI)$$

$$AR_2^2 + BR_2 + C = Z_2 \qquad (7BII)$$

$$AR_3^2 + BR_3 + C = Z_3 \qquad (7BIII)$$

The unknowns in the three equations are the polynomial coefficients A, B, and C which must be the same in each equation. By using Cramer's rule on the system of linear equations for A, B, and C each polynomial coefficient can be found. The general quadratic equation which results, Eqn.(8B), will give the correct axial distance for each radial value entered into the equation.

$$AR^2 + BR + C = Z \qquad (8B)$$

Subroutine Lift describes the lift-off phase of the arc formation and rundown. Once the current reaches a critical value the current sheath will expand radially outward to the outer electrode radius. This subroutine uses the equation of motion given by Eqn. (5B) to calculate the radial velocity. The change in radial position for the time increment is then found and added to the prior radial position. Inductance and inductance per unit time can then be calculated and passed back for use in the circuit equation.

Once the current sheath radially expands out to the outer electrode radius the Rundown subroutine is used to model the arc movement. To account for the change in electrode radius the quadratic equation generated from subroutine Cramer (eq. 8B) is rewritten in the form of:

$$R = -\frac{B}{2} \pm \sqrt{\frac{B^2}{4} - A(C - Z)} \qquad (9B)$$

If-then statements are used to determine which radial value is the correct one for the electrode. Once this is found, the computed radial value is used as input to calculate the axial velocity, inductance per unit length, and the inductance per unit time.

The previous version of the code utilized Eqns. (5B)&(6B) in the rundown to calculate inductance and inductance per unit length. In Eqns. (5B)&(6B) the inductance is independent of the step size of the axial rundown. Thus they are only valid for electrodes of constant radius since any change in the radius changes the radius of the entire electrode length. To account for radius changes in a stepwise manner, Eqn. (6B) was rewritten as:

$$L_{rd_{(n+1)}} = L_{rd_{(n)}} + \frac{\mu_0}{2\pi}(V_Z)H \ln\left(\frac{R_{out}}{R_{in}}\right) \qquad (10B)$$

Where

$L_{rd_{(n)}}$ = Inductance of previous rundown step

(V_Z) = Axial velocity

H = Time increment

Equation (10B) maintains a constant radius for only the length of the axial rundown step size. Accuracy of the equation is limited by the time increment H and the axial velocity V_z which is calculated from Eqn. (3B). Greater accuracy can be achieved by decreasing the time increment. The radius of the current sheath (RPR) had to be modified to include the additional arc length from the change in radius. This performed by adding Eqns. (11B)&(12B) which find the change in radius and adds it to the current length (RPR).

$$\Delta R_{(n+1)} = 2.54 - R_{in_{(n+1)}} \qquad (11B)$$

$$\Delta RE_{(n+1)} = \Delta RE_{(n)} + \Delta R_{(n+1)} \qquad (12B)$$

Where

$\Delta R_{in_{(n+1)}}$ = Radius of inner electrode at this increment

$\Delta R_{(n+1)}$ = Change in arc length

$\Delta RE_{(n)}$ = Distance between electrodes (arc length) at given increment

$\Delta RE_{(n+1)}$ = (RPR) = radius of current sheath = radius between electrodes

The axial velocity, axial position, inductance, arc length, and inductance per unit time are passed onto the main program where they are used in the circuit equation and other calculations.

The program structure of the main body consists of dividing the formation of the arc and the rundown into two parts. Initial conditions and parameters are set at the beginning and values for the electrode surface are entered. Subroutine Lift is called by the main loop while the current sheath is forming and is radially expanding to the outer electrode radius. Once the arc length reaches the outer electrode radius the program calls up subroutine Rundown which models the rundown of the arc between the electrodes. Each subroutine has no internal loops and the values of the inductance and inductance per unit length calculated in the subroutines are used as input for the circuit equation. The circuit equation for the system is solved by a fourth order Runge-Kutta method. Toward the end of the program the time step is advanced and different circuit values are written in a file. The program terminates once the arc rundown reaches the end of the inner electrode.

Appendix C

Advanced Gas Puff Valve Concept

Appendix C

Advanced Gas Puff Valve Concept*

Introduction

Rockford's Dense Plasma Focus (DPF) facility is dedicated to space propulsion studies. One thruster scheme [1] suggests discharging a 1 MJ capacitor bank into a DPF thruster at 10 kHz rate, producing 20,000 lb thrust. The short DPF event duration (3 μsec, compared to several μsec in conventional plasma guns) requires a very fast and accurate gas injection scheme. Gas injected too early or too late does not contribute to the thrust, thereby reducing the system's specific impulse.

The gas injection system design must meet three basic criteria [1]: First, an azimuthally uniform flow is required around the insulator, where the current sheath is formed. Second, the gas flow between the electrodes must enter preionized into the interelectrode gap. Third, a predetermined gas amount must flow as quickly as possible from the reservoir to the desired location.

The Rockford DPF group has designed an electrical solenoid gas puff valve based on the above requirements. As shown earlier in Fig. 11, a cylindrical gas injection port at the base of the insulator and the outer electrode serves as a flow distribution system. The predetermined mass flows from a cylindrical plenum, normally sealed off by a cylindrical flow restrictor, into the injection port. The plenum is initally filled to a predetermined pressure by opening four gas valves for a sufficient time, to ensure equilibrium before triggering gas injection. At triggering, the flow restrictor is opened simultaneously by four electromagnetic solenoids located above the plenum and inner electrode and pushed back by four springs, when the voltage is turned off.

A computer controlled electrical system, designed and constructed by Rockford, synchronizes the sequence of events for a single shot cycle. First, the restricting valve is opened, then the Marx generator is triggered followed by close command to the restrictor.

In the next section, we describe a preliminary analysis of the present gas puff system. The analysis used circuit solver as well as a Fortran code for the flow restrictor dynamics. Some alternative schemes which appear more

*Full version, including code write-up published earlier as Rockford Technology Report RTA-PF-03.

compatible with DPF thruster requirements are then presented and briefly analyzed. Finally, a discussion of the results and suggestions for future work are given.

Injection system modeling

The injection system may be simulated as a reservoir connected to a large volume, initially at vacuum, through an orifice, an annular pipe and another orifice (see Fig. C-1). The flow system characteristics are listed in Table 1.

Table C-1. The DPG Gas puff injector parameters

a. Flow system	
Cylindrical plenum volume	150 cm^3
Initial plenum pressure	50 Torr
Orifice circumference	22 cm
Annulus area and length	7.4 cm^2, 5.8 cm
Injection port area	15 cm^2
Inter-electrodes volume	1200 cm^3
b. Mechanical system	
Flow restrictor mass	0.5 kg
Spring constant (assumed)	$5x10^4$ N/m
Dampening factor (assumed)	0.1 N-sec/m
Initial spring compression	1 mm
Initial O-ring compression	0.18 mm
Force - 4 solenoids	165 N
Maximum restrictor stroke	2 mm

We assumed a constant solenoid force and ignored the catalog data, as explained below. The restrictor mass include the connecting rods and the solenoid anchors. The dampening factor accounts for the air compression during the restrictor movement.

First, one has to determine the flow regimes in the various segments of the flow system. Clearly, during the injection cycle, the flow changes from molecular to intermediate to viscous in all segments. A major problem simplification may result if the first two flow regimes can be neglected. The limits of the three flow regimes are:

Flow regime	Conditions
Viscous	$Q/D > 200$ $D/\lambda > 110$
Transition	$Q/D < 100$ $1 < D/\lambda < 110$

where D is the equivalent segment diameter in cm, Q is the total flow rate (Torr-lit/cm^2), and λ is the collisional mean free path.

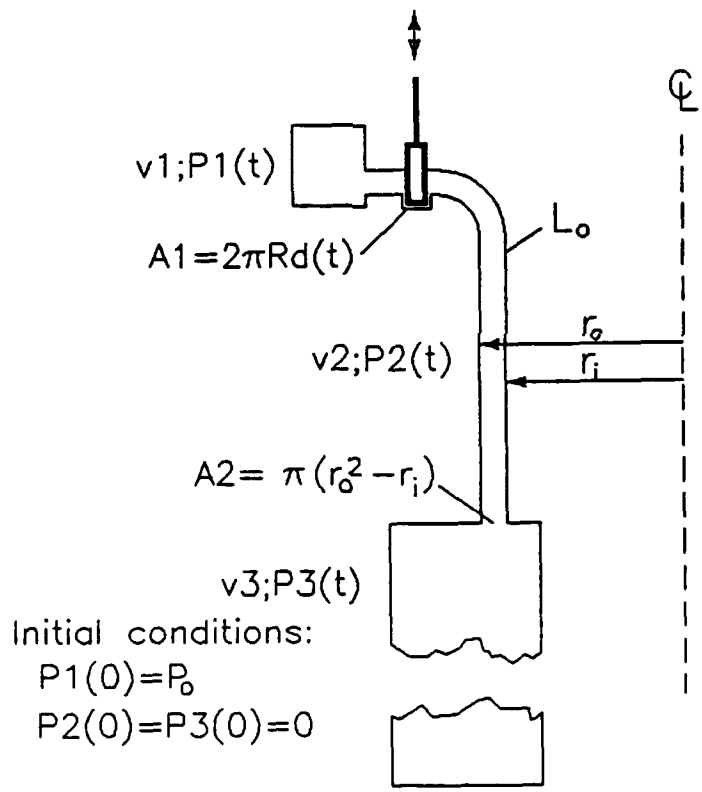

Figure C-1

Flow diagram for gas puff system.

With these inputs we can construct a simple model for the gas injection system. The viscous conductance C_v of a radial orifice is given by the approximate equations:

$$C_v = \frac{9.1\ A}{1 - (P_2/P_1)} \left[\frac{P_2}{P_1}\right] \left(\frac{2\gamma}{\gamma - 1} \left(\frac{T}{M}\right) \left[1 - \left(\frac{P_2}{P_1}\right)^{\frac{\gamma - 1}{\gamma}}\right]\right)^{0.5} \quad (1C)$$

Here C_v is the conductance in Torr-lit/cm^2, and P_1 and P_2 are the plenum and annulus pressures, respectively, $A = L_1 * d(t)$ is the orifice cross section while L_0 and $d(t)$ are the orifice circumference and gap, respectively, and M is the molecular weight of the gas. Note that the gap spacing is a function of time. The gas conductance of C_g the annular channel is given by the equation:

$$C_g = 900 \quad \frac{T}{M} \quad \frac{P}{L} \left[r_o^4 - r_i^4 - (r_e^2 - r_i^2) \log(r_o/r_i)\right] \quad (2C)$$

Where r_o, r_i, and L are the outer radius, inner radius, and annulus length respectively. The viscous conductance C_3 of the annulus end facing the inter-electrode gap may be found from equation 1C. The total flow system conductance C_T is calculated from the discrete C values:

$$C_T = \frac{1}{\sum_{i=v,g} \frac{1}{C_i}} \quad (3C)$$

The pressures at the three sections are calculated by integrating the net flow rate through each section. To complete the model, the annulus exit pressure is back-calculated from the flow rate through the exit orifice. The gap spacing d(t) is calculated by integrating the differential equation for the mass-spring system of the flow restrictor, with the initial conditions specified in Table 1:

$$\frac{dx}{dt} = M_r \frac{d^2x}{dt^2} + C \frac{dx}{dt} + K\ x(t) = F(t) \quad (4C)$$

A Fortran code has been constructed to simulate the pressure history in each segment. The inter-electrode volume is taken as a closed segment. This is a good assumption since the injection period is smaller than the gas (Fig. C-2b, C-2c). The pressure peak in the annulus is caused by the limiting chocked flow at the injection port. After a 7 msec transient, all segments reach pressure

equilibrium, before the gap is completely open at t = 10 msec.

An initial parametric study was conducted with the opening time set to about 250 μsec (simulating an arbitrary quick valve). As seen in Fig. C-3, the injector response time is longer than 1 msec, even if the annual segment reaches pressure equilibrium within a few 100's μsec. In other words, the present design requires additional iterations before becoming compatible with high rep-rate operation.

The present gas puff design incorporates four commercial solenoids supplied by a 110-V, 60-Hz utility line. Each solenoid rated pull force ranges from 40 to 20 Nt for 1/8" and 7/8" stroke respectively. However, due to the random phase (input voltage phase angle at switching onset) the solenoid current history is also random.

We made some preliminary runs using PSPICE circuit solver [3] and the circuit is depicted in Fig. C-4. The solenoid inductance ranges from 400 to 200 mH for zero and 1" stroke, respectively, but was taken as 200 mH. As predicted, the initial current (first 7 msec) depends on the initial voltage phase and reach 1.4 and 2.2 A for phase shifts of 90^{o} and 0^{o}, respectively. Since the solenoid's pull force is proportional to I^2, it may reach 80 Nt instead of 40 Nt and its performance as a repetitive valve driver may not be reproducible.

Discussion

Some improvements are required to upgarde the present injector to a high rep-rate device. The present Marx generator jitter (15 msec) plus the injected gas mass and timing variations seem to be inappropriate for such delicate plasma experiment. Even after correcting these problems, the present system could be operated at 20 Hz at best.

The random phase effect could be partially corrected by connecting an appropriate capacitor (50 uF for 200 mH) in series to each solenoid or by using a dedicated pulsed power supply. The DPF group has started initial efforts in the latter direction. The Marx generator jitter could be eliminated by one of the following routes:

- Triggering the Marx generator spark gap with an auxiliary small SCR/ferrite circuit [5].
- Replace the Marx generator with the thyratron/ capacitor bank (30 kV 0.03 uF) cabinet. This device seems to have sufficient energy to trigger the main spark gaps. The peak output voltage could be

FSL-91-111

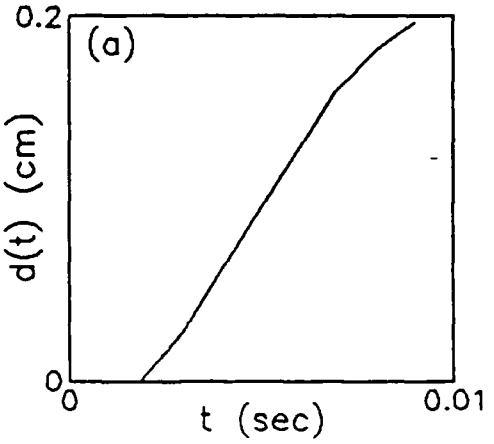

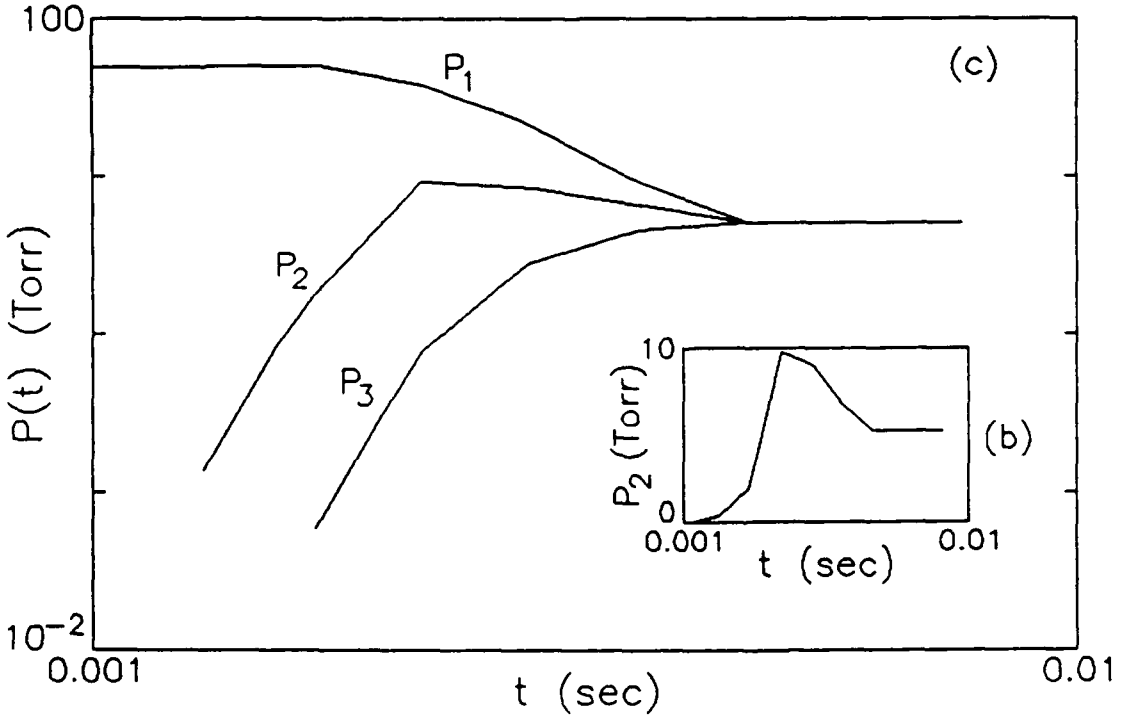

Figure C-2

Pressure histories in the present U of I flow systems:
(a) restrictor orifice gap
(b) annulár channel pressure (linear)
(c) pressure histories in all sections (logarithmic)

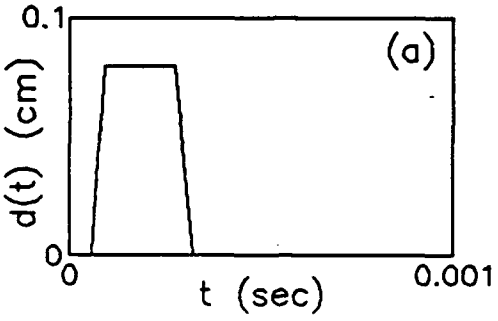

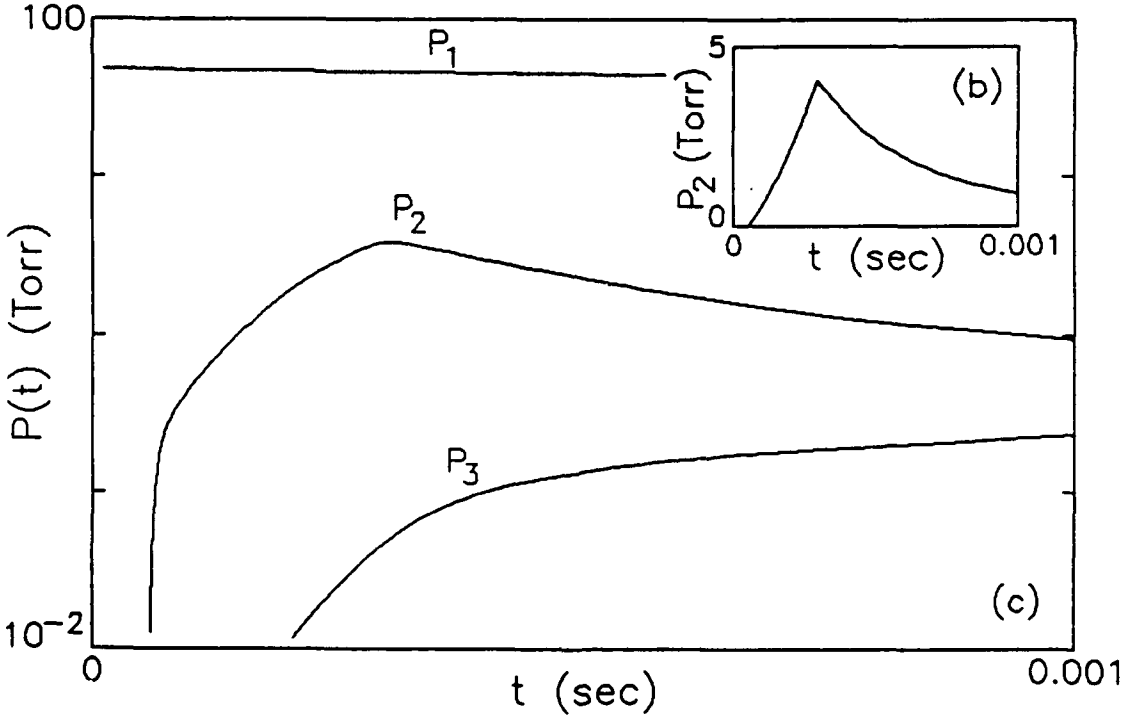

Figure C-3

Pressure Histories in a Hypothetical Piezo-motor Valve:
(a) valve opening
(b) annual channel pressure (linear)
(c) pressure histories in all sections (logarithmic)

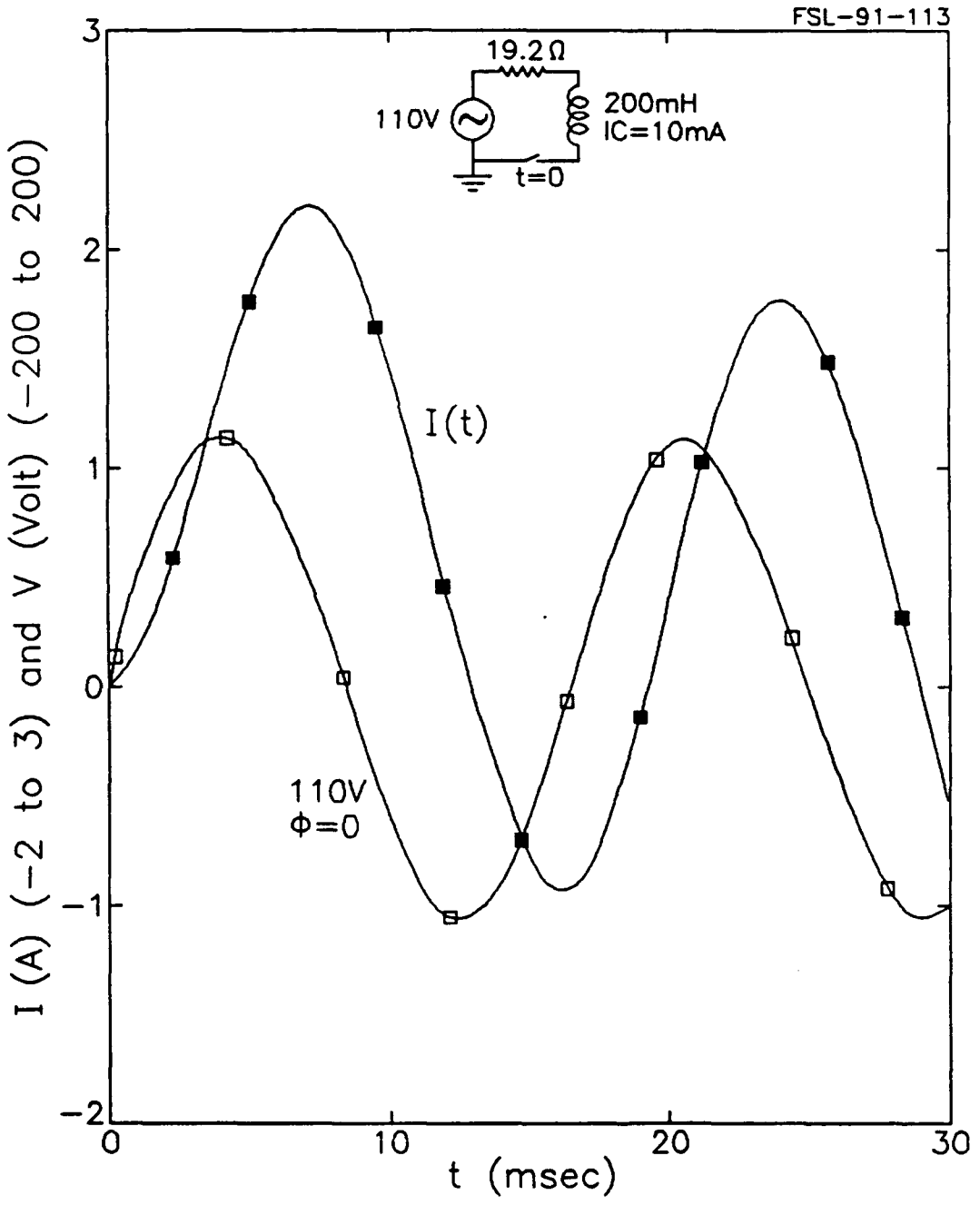

Figure C-4

Transient voltage and current traces - flow restrictor driver.

amplified if required, by using a double coaxial cable arrangement [4].

Apparently, a different gas puff system design would be appropriate for 1 kHz operation. One needs to increase the gas pressure in the plenum, and the charging rate, without changing the stored amount. One interesting approach is suggested in Ref. 5, which describes a 1 kHz magnetically insulated diode. A pre-determined gas amount is first allowed into the plenum using a foil diaphragm. In turn, the gas is inductively broken down, and MHD pushed into the plasma chamber. The MHD force accelerates the injection throughout, enabling the fast repetition rate.

The present computer controlled timing circuit developed by the DPF group is a powerful instrument that could be adopted to any gas puff injection scheme. However, a lesson to be learned from Ref. [7] is the danger of strong RF noise associated with the DPF system. An optical isolator could be installed between the computer control cables and the injection system to protect it against RF surges. This seems especially desirable at higher bank energies.

In summary, we analyzed the present gas puff system for the DPF using a Fortran computer code and the PSPICE circuit solver. The results indicate that the injection system requires some design modifications for use with banks with high energies and for scaling to high repetition rates. Repeatable injector performance would be achieved by using a phase sensitive trigger circuit or a dedicated pulsed power supply for the solenoids. The main spark gap trigger system would require re-design as well. We recommend protection of the injection system computer with an optical isolator.

References

1. B. Temple, O. Barnouin, and G. H. Miley, "Plasma Focus Device for Use in Space Propulsion," 9th Top. Meeting Technology of Fusion Energy, Oak Brook IL (October 1990).

2. Vacuum Technology, Pergamon Press, (1985), p. 60-65. (Engineering Library).

3. PSPICE version 3.03 User Manual, MicroSim Corp. (1987).

4. Pulsed Power Technology, Prentice Hall, Vol. I (1970) p. 55-80. (Physics Library)

5. W. A. Noonan, S. C. Glidden, J. B. Greenly, D. A. Hammer et al., "Operation of an Intense Ion Beam Diode at High Repetition Rate," IEEE Proc. Int. Conf. Plasma Science, Buffalo NY, (May 1989).

6. H. C. Harges, E. E. Kunhardt, M. Kristiansen et al., "Space-Charge Effects in a Laser Fiber-Optics Triggered Multichannel Spark Gap," IEEE Trans. Plasma Sci. PS-10 (4), p. 261-265 (1982).

7. T. Sato, I. Ochiai, Y. Kato, and S. Murayama, "High-Frequency Oscillations of Current and Voltage in a Plama-Focus Discharge Device," Rev. Sci. Instrum. 62 (6), p. 1504-1510 (1991).

Appendix D

Solid Target for DPF Thrusters

Appendix D

Solid Target for DPF Thrusters*

Introduction

Magnetoplasmadynamics thrusters (MPD's) have long been studied for space propulsion. Their exceptionally high specific impulse make them attractive given a spaceborne compact and safe electrical source. Deep space missions, however, require even better performance which could be achieved by fusion energy [1]. The Dense Plasma Focus (DPF) can serve as a plasma thruster and possibly as a fusion device with a scientific break-even $n\tau$ 10^{14} sec/cm^3, T_i = 10 keV capability. The better understanding gained recently on the DPF physics enables one to propose and analyze new schemes which may lead us to this goal.

DPF's and linear Z-pinches, have been of interest for controlled fusion research for three decades or more. Many studies suggested that these devices could form a very compact, high-Q fusion system. Indeed, several DPF's and Z-pinch fusion schemes were tested and these include:

1) Sub-MJ DPF without magnetic stabilization.
2) Z-pinch of laser preionized channel in dense deuterium-gas.
3) Z-pinch of a frozen deuterium fiber.

Several groups that did extensive experimental work on the first topic concluded that a peak current of 10 MA is required to achieve ignition [2]. However, recent DPF tests using an explosive generator did not produce a remarkable fusion event. Some laser initiated Z-pinch targets reached impressive $n\tau$ = 2x10^{12} sec/cm^3 at 299 eV. However, these values represent surrounding gas accretion resulting in higher core density but much lower core temperature (i.e., no fusion).

The frozen fiber approach is free of accretion but the results were disappointing. A detailed numerical study conducted at LANL [4] on the NRL frozen fiber experiment indicates peak core compression to 4X liquid density but the temperature remains below 1 eV, with a little magnetic field penetration. Once the fiber is completely ablated, its density profile turns promptly into a current carrying channel profile and the confinement is lost. A follow-up 2-D study [5] revealed early (t = 20 nsec) loss of confinement due to large scale m = 0 instability.

Brownell and Freeman [2] suggested to implode a gaseous DPF onto a pressurized DT filled glass target. This arrangement would serve as an "impedance match" between the available energy and the fuel. Their 1-D radiative-

hydrodynamics calculations indicate that the fuel temperature and density peaks become synchronous in this way. Their predictions indicate lower fusion yield from these targets compared to experimental results in ordinary non-stabilized DPF. Gratton et al., [3] suggested imploding an ordinary DPF on fusionable fibers. Their scheme is to shock-ionize the fiber by the imploding focus and to divert the current flow from the imploded focus into the dense core, hoping to achieve $J_s x B_\theta$ confinement. Unfortunately, the compressed target might ablate and expand as the frozen fiber, before reaching a confinement current level.

The above DPF-target proposed schemes overlooked the possibility to spark ignite the core using instabilities originated by hot ions. Indeed, the energy-weighted DPF generated ion beam range within a 10X length/diameter ratio (10X L.D.) in the dense D-T plasma is only a few 100's of microns. On the other hand, the total beam's energy may bring the target core to fusion temperatures. For example, the energy imparted to the hot ion beam in a typical POSEIDON DPF experiment [6] represents about 1% of its 0.4 MJ capacitor bank.

In this proposal, we introduce a new target design for DPF-target experiments. The new approach utilizes inertial confinement through momentum transfer from DPF as in Ref. [2], plus, a stabilizing axial magnetic field (i.e. thermal insulation), and "spark ignition" of a hollow foamed fusionable target utilizing deliberate instability originated hot ions. The next section describes a basic analysis of the proposed scheme. More detailed analysis using a modified 0-D code is described in Section III. Discussion on the results and the ion beam heating is included in the last section.

Fundamentals

Following the above review, a hollow thin walled target such as shown in Fig. D-1 has been selected as the first iteration target geometry. For optimal momentum transfer, the imploded DPF and target masses must be comparable. A 5-cm, 10-Torr, D-T gas layer is equivalent to a 0.8-μ liquid D-T layer. From a dimensional stability point of view, a foamed-wall hollow target saturated with liquid D-T appears more realistic than a pure frozen D-T layer [7]. The hollow target radius is optimized such that the imploded DPF would approach its full radial velocity and the magnetic field diffusion time would be maximized.

After elastic collision with a hollow target, the foamed target averaged implosion velocity varies according to the following equation:

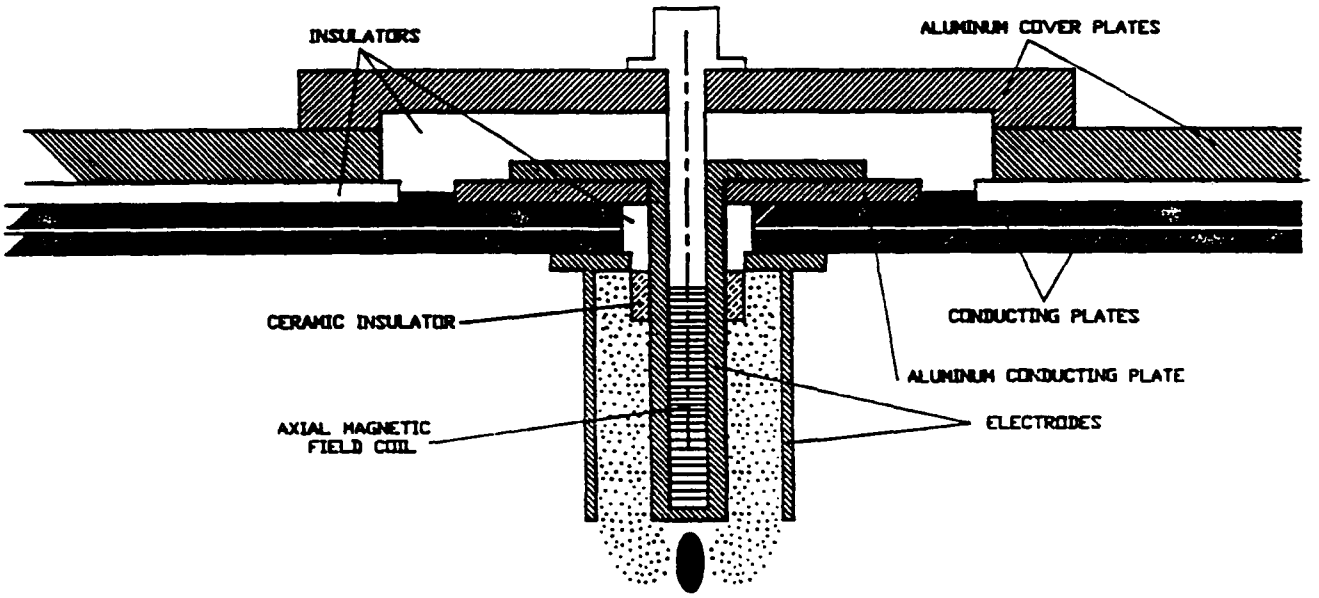

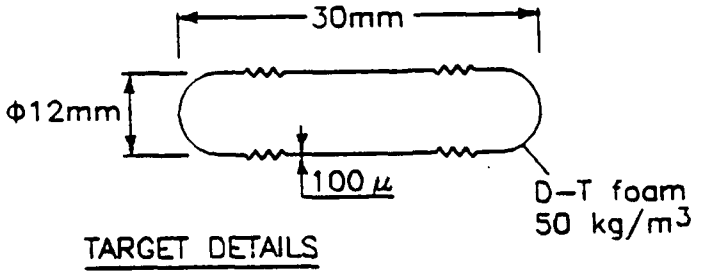

Figure D-1

The hollow foamed target concept.

$$V_f = \frac{V_p M_p}{M_p + M_f} \cdot \qquad (1D)$$

Figure D-2 illustrates the variation in the compressive ($J_z x B_\theta$ and hydraulic ram) and back pressure (B_z and plasma pressure) components during the foamed target compression, neglecting radiative losses. The compression and pressure components equilibrate at about $r = 0.1 r_p$, while the target density increases from 50 kg/cm^3 to about 16X L.D.

The results explain also the "matching" mechanism [2] between the imploded DPF and the target: The hydraulic ram pressure reduces the compressing target radius to a point that the $J_z x B_\theta$ force can take over and further increase the target density. It is interesting to note that although B_z reaches 32 T at peak compression, its contribution to the back pressure is negligible at peak compression. On the other hand, a complete control over the m = 0 instability would be gained by such B_z magnitude. If hot ions are generated, a 32 T axial field would be capable of diverting many ion trajectories onto the dense target core.

Because of its simplicity, the above procedure may also be also used to predict the target parameters effect on the peak fuel density. Table D-1 lists the peak fuel density vs. wall thickness for the target cited above. The implosion velocity is calculated for each case using Eqn. (1D).

Table D-1. Peak ρR and Density vs. Hollow Target Wall Thickness.

Wall thickness microns	peak ρR mgr/cm^3	Peak density (L.D.)
10	14	16.
20	14	7.7
30	13	4.3
50	12.5	2.3
100	12	1.1

For comparison, the peak density of the same DPF without a centered target is rather low. For the initial conditions: I_z = 1 MA, $v_{1mp} = 6 \times 10^3$ m/sec, ϕ = 0.01 Kg/m^3. T_e = 5 eV, the peak core density at equilibrium (assuming no instabilities) is 0.8 Kg/m^3 or 0.004X L.D. The contribution of the "pressure components" is shown in Fig. D-3. Similar phenomena occur in multi-stage compressors with intermediate heat exchange, where final gas density is much higher for the same power input.

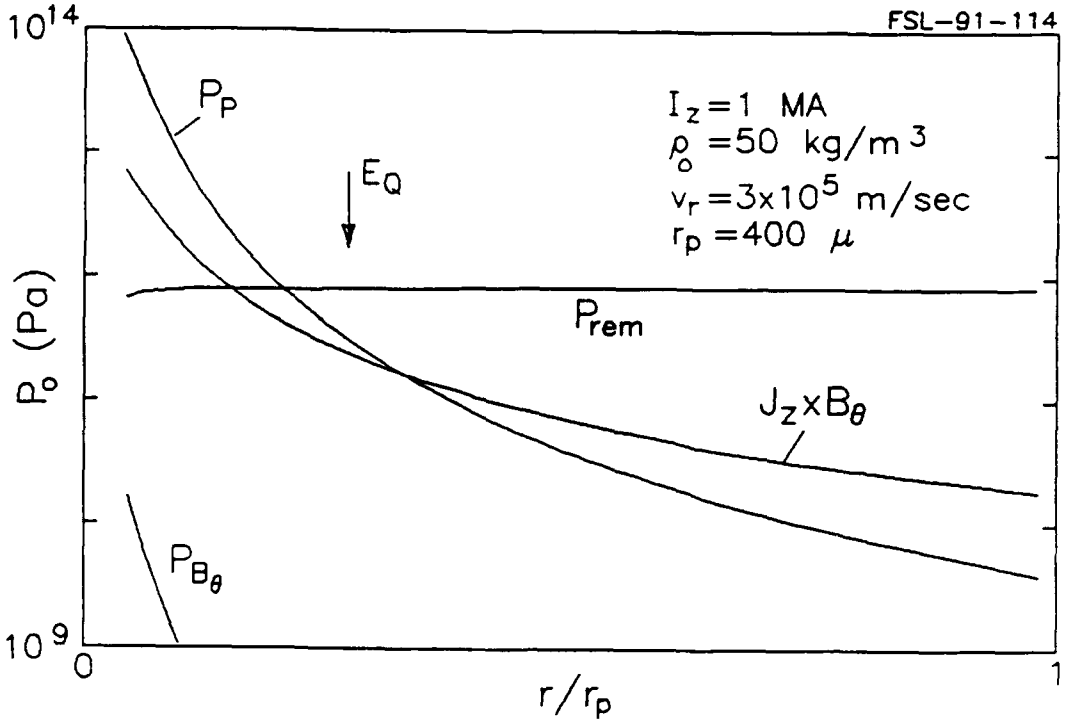

Figure D-2

Pressure and compression components variations during hollow target compression.

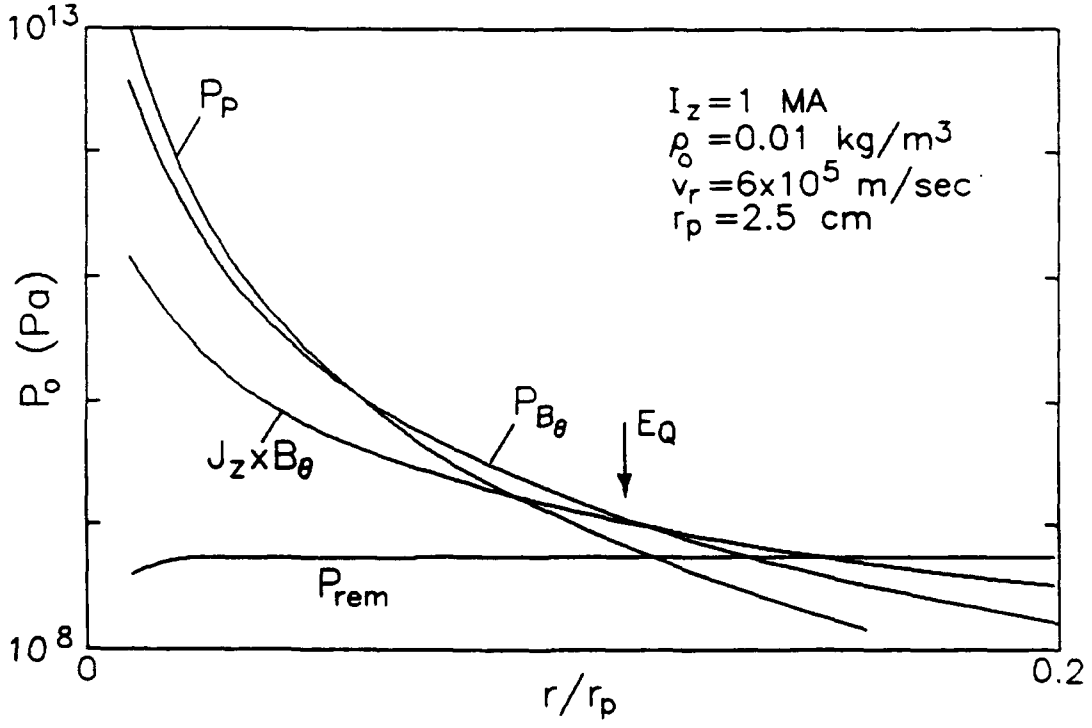

Figure D-3

Pressure and compression components variations during gaseous DPF event.

Extended 0-D model

The scoping study used in the previous section does not time integrate and thus cannot be utilized to predict important implosion data such as the confinement parameter. In addition, several key processes such as radiative cooling and target rebounce are ignored. Still, this study provided vital information about the work point and the energy matching process.

Where M_p and M_f are the imploded DPF and foamed target masses while V_p and V_f and the DPF and foamed target radial speeds at collision, and p is the sum of plasma and axial magnetic field pressure. For $V_f = 3 \times 10^5$ m/sec and target radius $r_f = 0.8$ cm, the DPF-target contact time is about 20 nsec. We assume that average axial magnetic field at the target wall is about 10% of the DPF's envelope field. During compression, the average axial magnetic field B_z increases according to the equation:

$$\frac{dB_z}{dt} = -\left(\frac{r_0^2 \, B_{z0}}{2 \, r^3}\right) \frac{dr}{dt} \qquad (2D)$$

Where B_{z0} and r_0 are the average magnetic field and target radius at compression onset.

Assuming negligible target preheating from the DPF's hot electrons, the foamed target wall will maintain its density after gaining momentum from the imploding DPF. Therefore, at the onset of void closure, the imploded foamed target radius, r_p will be:

$$r_p = \sqrt{2 \, r_0 \, \delta r} \qquad (3D)$$

During compression, the radial velocity is governed by the difference between the compressive and internal forces. The variation of each component with radius is described in the following 0-D approximation:

$$P_{JB} = \frac{\mu_e \, I_z^2}{4 \, \pi^2 \, r_p^2} \qquad (4Da)$$

$$P_{rem} = \frac{M_f \, V_f^2}{6 \, \pi \, 1_0 r_p^2} \qquad (4Db)$$

$$P_p = k \, (n_e \, T_e + n_i \, T_i) \qquad (4Dc)$$

$$P = \frac{B_z^2}{8 \pi \mu_0} \qquad (4Dd)$$

In order to obtain a better insight into this problem we have written a simple Fortran code which integrates the forces acting on the cylindrical target along the compression path. The initial target conditions are listed in Table D-2.

Table D-2. Initial Conditions for An Imploded Foam Target.

Total current through target	1 MA
Imploded target radius	400 μ
Foam density	50 kg/m^3
Initial B_z	0.5 T
Implosion velocity	3×10^5 m/sec
Target temp. before compression	1 eV

For the present proposal we selected the 0-D MHD integrator written by F. Venneri for his PhD. thesis at the U. of Illinois [8]. This code uses fourth order Runge Kutta integration scheme for the circuit equations and a three stage 0-D DPF dynamics model. A constant axial velocity is assumed for the lift-off and run-down phases. The 0-D model for the compression phase uses an ideal gas snow-plow model suggested in Ref. [9]. The model includes anomalous resistivity, magnetic field compression and diffusion, and a simple ionization-radiation model. The code output includes the DPF outer radius, averaged temperature, pressure, density and axial magnetic field.

We have modified the code to enable insertion of a solid target during the collapse phase. When the inner DPF surface collides with the foamed target, the latter's implosion velocity is calculated assuming an elastic collision. A one group radiation transport model has been added to the code using total emission data assuming an optically thin region. The current is assumed to flow through the imploding target wall. The adiabatic exponent is plasma density. The circuit is simulated such that one capacitor bank drives the DPF while a larger bank is discharged onto the imploding target.

Initially we successfully tested the modified code with the initial conditions used in Ref. [10]. Then we conducted runs to estimate the optimal DPF-target collision radius (0.8 cm, from maximum velocity - maximum contact time optimization). From these calculations, initial parameters were selected for the DPF and target as listed in Table D-3.

Table D-3. Initial Conditions for DPF and Target Implosion.

	DPF	Target
Capacitor bank	100 kJ, 60 kV	900 kJ, 60 kV
Fuel density	0.01 kg/m^3	50 kg/m^3
Outer radius	5 cm	0.8 cm
Wall thickness	2.5 cm	20 μ

The results of this run are depicted in Figs. D-4a-f. The peak density and temperature are 4X L.D. and 700 eV respectively compared to 7.7 L.D. predicted in Section II. The confinement time is estimated as 4×10^{13} sec/cm^3 and the averaged R is 10 mgJ/cm^2. We attribute the lower density to target elongation and prompt loss of the hydraulic ram pressure at void closure predicted by the 0-D code. The peak compression time lasts about 500psec while the discharge current decreases due to the I_z dL/dt term in the circuit equation. Testing the same configuration with ρ_{13} = 70 kg/m^3 gave a peak density and $n\tau$ of 6X L.D. and 8×10^{13} sec/cm^3, respectively. As opposed to gaseous DPF events, this remarkable confinement parameter is possible during the first compression phase only.

Discussion

The attractiveness of DPF as a thruster could be enhanced even further by generating a thermonuclear burn in a solid target placed on-axis. Achieving an intermediate goal (e.g. 5×10^{17} D-T fusion events for 1 MJ input) would justify this approach over Marshal gun or other non-imploding plasma guns.

The hollow, foamed target has a two-fold advantage over a solid target. First, the pinched target carries a stabilizing axial magnetic field and second, the compressed core temperature is initially higher, improving the chance for thermonuclear ignition. An overall view may be obtained from Fig. D-5, which illustrates various DPF compression schemes on the radius-density plane. The extended constant-density collapse period, which is unique for this target configuration, enables one to implement magnetic stabilization and hot ion generation.

The 0-D code predictions appear to be in good agreement with the preliminary analysis: The insertion of dense hollow target into the DPF enable very high peak target density with an impressive confinement parameter (4×10^{13} sec/cm^3).

The physics of magnetic field stabilization was briefly studied in the present work. A 2-D numerical analysis [5]

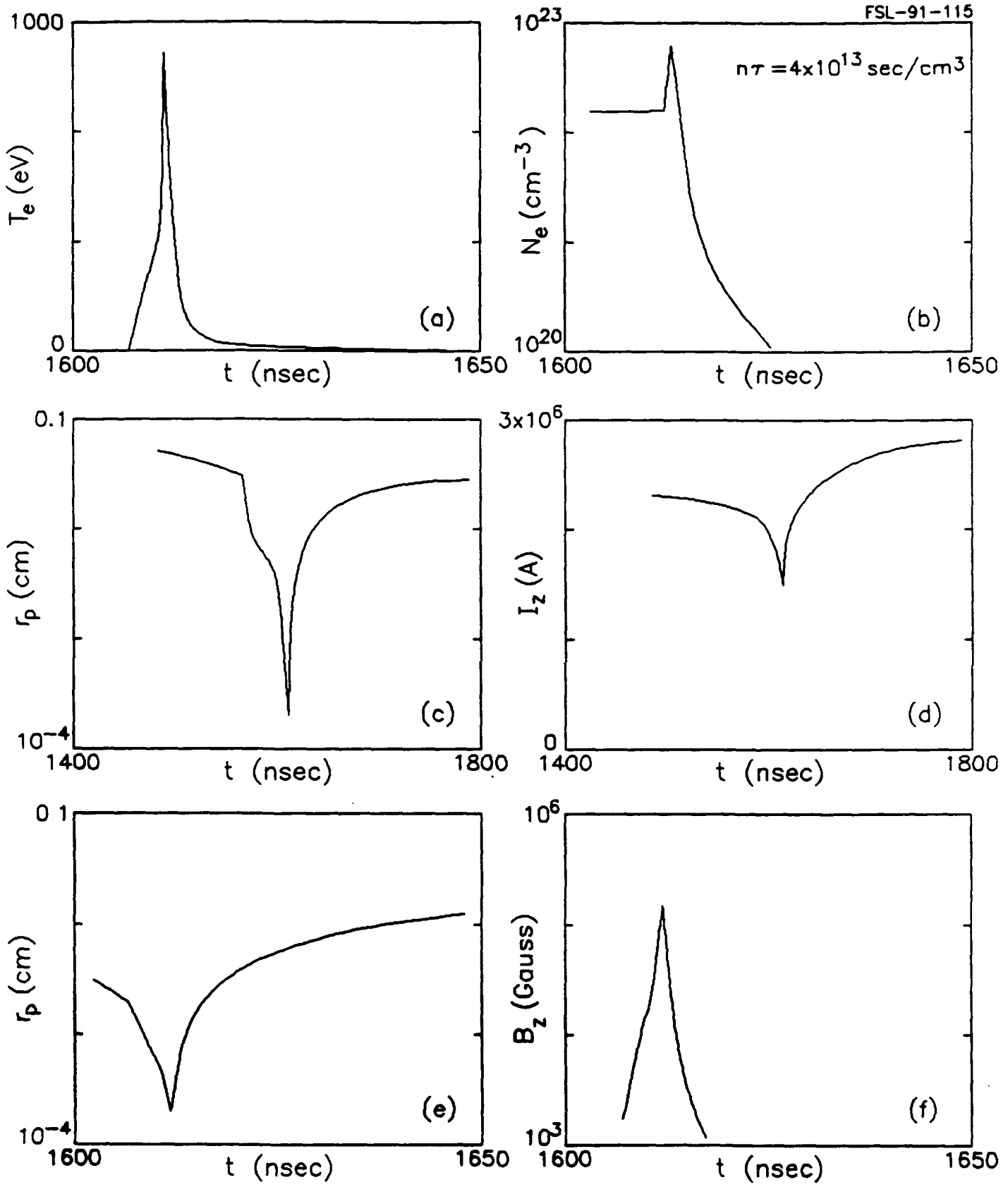

Figure D-4

The modified 0-D code output. (a) Electron temperature, (b) Fuel density, (c) Target radius, (d) Axial current, (e) Target radius (magnified), (f) Axial magnetic field.

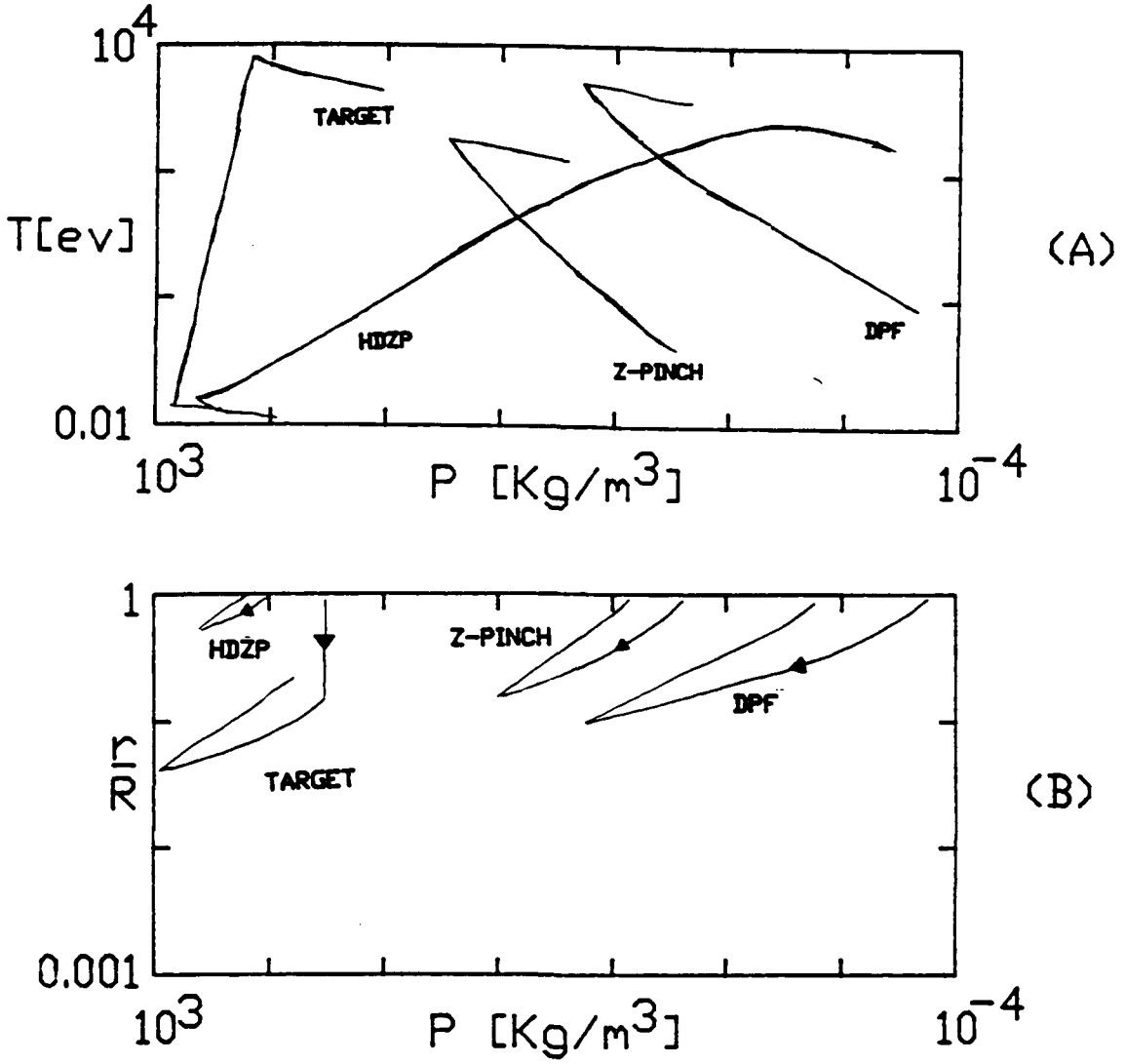

Figure D-5

Comparison of various cylindrical implosion schemes (pure D_2) Target = present concept; HDZP = high density z-pinch; DPF = dense plasma focus. Fig.(a) plots T vs. P while (b) shows the radius r vs. P.

demonstrates how a dense solid Z-pinch is disrupted by the m = 0 instability. Several experiments, scattered in the density-confinement time plane [11], do indicate that magnetic field stabilizes the implosion and extends the confinement time.

As predicted above, the compressed core is at sub-keV temperature while the hot ion generation mechanism is suppressed by the stabilizing axial magnetic field. Therefore, it is essential to identify a mechanism for "spark igniting" the core at its peak density (~500 psec period). The deutron beam energy sufficient for spark ignition is quite small. Heating 1% of the mass of the target in Table 1 to 5 keV requires only about 4 kJ. However, an efficient target burn requires that a 5-keV spark would simultaneously initiate along the target axis.

A detailed study on the hot deutron beam was conducted earlier on the 0.5-MJ DPF POSEIDON facility [6] (without magnetic stabilization). The deutron beam source distribution, energy spectrum, and source distribution were deduced from neutron yields, energy spectrum and charged particles pinhole images. During the first compression phase, about 50 J are released into 30 keV deutrons. During the unstable stage, however, significant energy (3 kJ) was routed into a 100 keV beam. The source distribution appears to be randomly scattered along the DPF's axis.

An earler study [12] on a magnetically stabilized DPF (0.12 T) indicates that the neutron output is reduced by one order of magnitude, but its spectrum remains the same. This data indicates that the energetic 0.2 - 1 MeV deutron flux is reduced by at least a factor of ten, while the intermediate (30 keV) ions suffer a smaller flux reduction. Furthermore, electric field accelerating the ions acquire a larger radial component. In terms of the present scheme, this would result in even lower core preheating.

In their effort to understand the Reileigh Taylor (RT) instabilities in ICF targets, the Laser group at Livermore engraved a few micron deep grooves on some microballoons to simulate the RT growth rate under various implosion conditions. Indeed, RT instabilities were obtained repetitively within the pre-groved target regions [13]. Thus the implosion of DPF target with grooves along its circumference would induce local m = 0-like instabilities at peak compression. Close examination of the DPF's unstable phase (Fig. 1 of Ref. [6] reveals severe expansion and contraction regions initialized by the m = 0 instability. The hot ions are emitted from the contraction sections at peak compression. These observations lead us to propose the use of a grooved target for the DPF.

In spite of the little theoretical support, previous experiments and theoretical studies suggest indirectly, that synchronized spark ignition of compressed DPF cores is possible. This could be done by generating deliberate instabilities in which hot deutron beams would be produced. The beam energy would be deposited favorably along the target's axis, due to the strong axial magnetic field. Furthermore, once a thermonuclear burn has been initiated, the field would enhance alpha particle energy deposition and sustain the burn until the target disintegrates.

In summary, we recommend use of hollow targets with circumferential grooves, since such targets should produce the hot ion production needed for spark ignition. In addition to the existing diagnostics, we suggest development of a hot ion "camera" consisting of a pinhole pattern combined with a spectral resolving X-ray filter array and a CR-39/pinhole combination [6]. Comparing the ion beams images with and without magnetic stabilization, would indicate the prospects of hot ion generation for the proposed scheme. Such preliminary experiments can be done on the 1/4-MJ module while a full target study would require the full 1-MJ bank.

V. References

1. B. Temple, O. Barnouin, and G. H. Miley, "Plasma Focus Device for Use in Space Propulsion," 9th Top. Meet. Technology of Fusion Energy, Oak Brook IL (October 1990).

2. J. H. Brownwell and B. L. Freeman, "Plasma Sheath Driven Targets," Appl Phys. Lett. 36 (3) p. 193 - 194 (1980).

3. R. Gratton, A. R. Piriz, and J. O. Pouso, Nuclear Fusion 26 p. 483 (1986).

4. I. R. Lindemuth, G. H. McCall, and R. A. Nebel, "Fiber Ablation in the Solid Deuterium Z-Pinch," Phys. Rev. Lett. 62 (3) p. 264 - 267 (1989).

5. I. R. Lindemuth, "Two-Dimensional Ablation in the Solid-Deuterium Z-pinch," Phys. Rev. Lett. 65 (2) p. 179 - 182 (1990).

6. U. Jager and H. Herold, "Fast Ion Kinetics and Fusion Reaction Mechanism in the Plasma Focus," Nuclear Fusion 27 (3) p. 407 - 423 (1987).

7. Laser Program Annual Report 87', Lawrence Livermore National Laboratory, Livermore CA, UCRL-50021-87 (1988). p. 4-23 - 4-33.

8. F. Venneri, "X-ray Analysis of a Dense Plasma Focus," PhD Thesis, University of Illinois (1988).

9. Y. Kondoh and H. Hirano, "Numerical Study of an Ion Acceleration in a Z-pinch type Plasma Focus," Phys. Fluids 21 (9) p. 1817 - 1822 (1978).

10. J. Mandrekas, "Zero-Model for the Dense Plasma Focus," MSc. Thesis, University of Illinois (1984).

11. R. C. Kirkpatrick and R. Lindemuth, "Ignition and Burn in Inertially Confined Magnetized Fuel," Proc. ICENES 91' Monterey CA (June 1991).

12. M. J. Bernstein and F. Hai, "Neutron Production in a Plasma Focus Discharge with and without Axial Magnetic Field," Phys. Fluids, 14 (5) p. 1010 - 1018 (1970).

13. Laser Program Annual Report 86', Lawrence Livermore National Laboratory, Livermore CA, UCRL-50021-86 (1987), p. 4-60 - 4-63.